

# Exploring an Alternative Channel of Evolution Towards SNa Ia Explosion

E. Chiosi<sup>1</sup>, C. Chiosi<sup>1,2</sup>, P. Trevisan<sup>2</sup>, L. Piovan<sup>2</sup>, & M. Orio<sup>1,3</sup>

<sup>1</sup> *Astronomical Observatory of Padova, INAF, Vicolo dell'Osservatorio 5, 35122 Padova, Italy*

<sup>2</sup> *Department of Physics and Astronomy, University of Padova, Vicolo dell'Osservatorio 2, 35122 Padova, Italy*

<sup>3</sup> *Department of Astronomy, University of Wisconsin Madison, 475 N. Charter Str., Madison WI 53706, USA*

*E-mail: emanuela.chiosi@oapd.inaf.it (EC); cesare.chiosi@unipd.it (CC); patrizia.trevisan@unipd.it (PT);*

*E-mail: lorenzo.piovan@gmail.com (LP); marina.orio@oapd.inaf.it (MO)*

Submitted: September 2014; Accepted: \*\*\*\*

## ABSTRACT

In this paper we explore the possibility that isolated CO-WDs with mass smaller than the Chandrasekhar limit may undergo nuclear runaway and SNa explosion, triggered by the energy produced by under-barrier pycno-nuclear reactions between carbon and light elements. Such reactions would be due to left over impurities of the light elements, which would remain inactive until the WDs transit from the liquid to the solid state. We devise a simple formulation for the coulombian potential and the local density in a ionic lattice affected by impurities and introduce it in the known rates of pycno-nuclear reactions for multi-component plasmas. Our semi-analytical results indicate that the energy generated by these pycno-nuclear reactions exceeds the WD luminosity and provides enough energy to elementary cells of matter to balance the energy cost for C-ignition at much younger ages than the age of the Universe, even for WDs with masses as low as  $\simeq 0.85 M_{\odot}$ . A thermonuclear runaway may thus be triggered in isolated WDs. The explosion would occur from few hundred thousand to a few million years after the WD formation in the mass interval  $0.85 - 1.2 M_{\odot}$ .

**Key words:** Stars – structure, evolution; White Dwarfs – pycno-nuclear reactions – Supernovae Ia

## 1 INTRODUCTION

Carbon-Oxygen White Dwarfs (CO-WDs) originate from low and intermediate mass progenitors in the mass interval  $0.7 - 0.8 M_{\odot}$  to  $6 M_{\odot}$  (Weidemann 1967, 1977, 1990; Chiosi et al. 1992; Weidemann 2000), which after the central H- and He-burning phases develop a highly electron degenerate CO core (electrons are fully degenerate and nearly relativistic). After the thermally pulsing AGB phase, these stars eject the whole envelope, baring the CO core. A WD is thus formed by a CO core surrounded by thin (if any) layers of lighter elements.

Given any reasonable initial mass function, about 97% of the stars of any generation with lifetime shorter than the age of the Universe ( $13.7 \pm 0.2$  Gyr according to Spergel et al. (2003)) end as WDs. Kepler et al. (2007) examined a sample of 7755 DA-WDs from the SDSS catalog and concluded that the vast majority of the 616 DBs and DOs listed in Eisenstein et al. (2006), fall in the mass interval  $0.5 - 0.7 M_{\odot}$ . The peak value is  $0.6 M_{\odot}$  and the range of masses extends from about  $0.4 M_{\odot}$  toward the low mass end to  $1.2 - 1.3 M_{\odot}$  on the opposite side. According to theoretical

models, there also is a clear relationship between the progenitor and WD masses,  $M_i$  vs  $M_{WD}$ , (Weidemann 1967, 1977, 1990; Chiosi et al. 1992; Weidemann 2000; Marigo 2001; Catalán et al. 2008) for which there is a plausible explanation based on current theory of stellar structure and evolution (see below for more details).

The most important facts of the WD theory are: (i) Except for a thin surface layer, the equation of state (EOS) can be approximated as fully degenerate electrons ( $P \equiv P_e$ ) with kinematic conditions changing from non relativistic ( $P_e = K_{5/3} \rho^{5/3}$ ) to fully relativistic ( $P_e = K_{4/3} \rho^{4/3}$ ) with increasing central and mean density. (ii) The structure of a WD of given chemical composition (mean molecular weight of ions and/or electrons,  $\mu_i$  and  $\mu_e$  respectively) is fully determined by its central density. (iii) Assuming Newtonian hydrostatic equilibrium, the WD mass has a maximum value, called the Chandrasekhar mass  $M_{Ch}$ , for which the central density is infinite so that the EOS is fully relativistic. In this case,  $M_{Ch} = 5.85/\mu_e^2$  with  $\mu_e$  the molecular weight of electrons. For a typical CO-WD,  $\mu_e \simeq 2$  so  $M_{Ch} \simeq 1.46 M_{\odot}$ . However, the radius of the Chandrasekhar mass is zero. Clearly such

non physical situation means that no WD can be born with the Chandrasekhar mass, which therefore is a mere ideal value. (iv) Along the sequence toward the Chandrasekhar value at increasing central density, two important physical processes can intervene, overall instability driven by General Relativity (GR) effects, and pycno-nuclear burning. WDs more massive than about  $1.3 M_{\odot}$ , i.e. denser than about  $3 \times 10^9 \text{ g cm}^{-3}$ , become dynamically unstable because of GR (Shapiro & Teukolsky 1983); C-O WDs denser than about  $6 \times 10^9 \text{ g cm}^{-3}$ , may start pycno-nuclear burning during the liquid-solid regimes (Shapiro & Teukolsky 1983). The onset of these phenomena may lead to a thermo-nuclear runaway. Therefore, all stable WDs we observe must have formed with masses lower than  $1.2 - 1.3 M_{\odot}$ .

The current theory of type Ia SNe assumes that the Chandrasekhar mass can be reached by accretion or merging and although the details are not fully known, carbon is ignited via the pycno-nuclear channel. This is followed by C-detonation or C-deflagration (the latter is more likely) and by a thermal runaway, because the gravo-thermal specific heat of the star is positive. The liberated nuclear energy exceeds the gravitational binding energy and the star is torn apart (see the recent review by Nomoto et al. 2013, and references therein). Binary models for type Ia SNe are classified as *double-degenerate*, i.e. the merger of two gravitationally bounded WDs, and *single-degenerate*, i.e. the evolution to the explosive phases is due to the accreting material from a companion star (see e.g., Napiwotzki et al. 2003; Trimble & Aschwanden 2004; Orío 2013).

Owing to the important role of the pycno-nuclear reactions in destabilizing a WD close to the Chandrasekhar mass and triggering type Ia SNe explosions, it is worth examining in some detail the condition under which pycno-nuclear reactions can occur. The pycno-nuclear regime starts in very dense and cool environments, i.e. in the liquid/solid state. While both the central and mean densities are determined by the WD mass and remain nearly constant if the mass does not change, the temperature decreases because the WD is radiating energy from the surface. Because there are no nuclear sources and the electrons are highly degenerate, while the WD radiates, the ions must cool down and transit from gaseous to liquid, and eventually solid (crystallised) conditions, i.e. carbon and oxygen ions form a lattice which is pervaded by a gas of electrons. As the temperature decreases, the ions eventually reach the fundamental energy state under a coulombian potential that approximately has the form of a harmonic oscillator. In quantum physics, the energy of the fundamental state of a harmonic oscillator is  $1/2\hbar\omega$  ( $\omega$  is the plasma frequency). This means that even at extremely low temperatures there is a finite probability for the C and O ions to penetrate the repulsive coulombian barrier. In this scheme, the rates of pycno-nuclear reactions between C and/or O ions were first calculated by Salpeter & van Horn (1969) and then refined over the years.

In their pioneering study, Salpeter & van Horn (1969) first noticed that impurities may enhance the pycno-nuclear reactions among the nuclei of the lattice. The enhancement is due to local over-densities in the sites of the impurities. Furthermore, even the contaminant nuclei themselves may react with the lattice nuclei, thus contributing to the total energy generation. If this happens, WDs that are less dense and/or less massive than the limits we discussed above be-

come unstable to the ignition of pycno-nuclear reactions triggered by impurities. Since at the distance scales corresponding to the densities of old WDs, electric forces dominate the scene, impurities due to light elements, such as hydrogen or helium, may induce higher local over-densities so that light elements can more easily cross the coulombian barriers.

In order to explore this idea, first we evaluate the change induced by the light element contamination on the typical inter-ion distance  $R_o$ . Second, we present the reaction rates in the pycno-nuclear channel for reactions like H+C, He+C, etc. Finally, we explore the possibility that even isolated WDs with mass significantly smaller than the Chandrasekhar limit and relatively low density (i.e. in the ranges  $0.85 - 1.2 M_{\odot}$  and  $10^7 - 10^8 \text{ g cm}^{-3}$ , respectively) may undergo nuclear runaway, because of the energy produced by under-barrier nuclear reactions by contaminant elements, when the WDs reach the liquid/solid state.

The paper is organized as follows. In Section 2 we first shortly review the history of a WD progenitor and the cooling and crystallization processes of ions in the WD, and introduce the relationships between the progenitor mass and the WD mass and between the WD mass and its central density. In Section 3 we describe the fundamentals of nuclear burnings in WDs, summarize two current sources for the reaction rates in both the thermal and pycno-nuclear regimes for single and multi-component fluids, and present a preliminary comparison of the reaction rates. In Section 4 we evaluate the changes in the rates due to impurities, first in the transmission probability of the coulombian potential barrier penetration and then in the local density. Since impurities by light elements are more efficient than those by heavy elements, in Section 5 we estimate the abundances of hydrogen and helium left over by previous evolutionary phases. After an initial phase at the beginning of the cooling sequence in which part of the energy may be of nuclear origin, for a long time the only source of energy is the thermal energy of the ions and all nuclear sources are turned off. Therefore the light elements remain inactive for a long time until the WD reaches the conditions for the activation of the pycno-nuclear regime. In Section 6 we estimate and compare the energy production by reactions like  $^1\text{H} + ^{12}\text{C}$  and  $^4\text{He} + ^{12}\text{C}$  showing that they can produce the typical luminosity of an old WD in the pycno-nuclear stage. In Section 7, we follow the evolution of WDs of different mass along their cooling sequences towards the pycno-nuclear regime and explore the effect of different abundances of light elements (H in particular) on the energy release by nuclear reactions. We estimate the abundance of contaminant elements and the epoch at which the nuclear energy generation first equals and then exceeds the WD luminosity. In addition to this we formulate a new condition for C-burning ignition in a liquid, semi-solid medium and propose a two-steps mechanism (named "*the fuse C-ignition*") for igniting carbon in elementary volumes defined by the mean free path of thermal conduction. For plausible values of H and He abundances, WDs with masses as low as  $\simeq 0.85 - 0.9 M_{\odot}$  (and above) reach the critical condition for rekindling the nuclear energy production and initiate a thermal runaway. Finally, in Section 8 we draw some conclusions about the possible implications of these results for the progenitors of type Ia SNe.

## 2 GENERAL PROPERTIES OF WDS

### 2.1 Evolution of the progenitors

The structure and evolution of low and intermediate mass stars, the progenitors of CO-WDs, can be described with the aid of three milestone masses (for all details see Iben & Renzini 1983; Kippenhahn & Weigert 1990; Chiosi et al. 1992). We define low mass stars those that develop an electron degenerate helium core, shortly after leaving the main sequence toward the red giant branch (RGB). When the mass of the He-core has grown to a critical value (0.45-0.50  $M_\odot$ , the precise value depends on the composition, star mass, and input physics), a He-burning runaway (called He flash) starts in the core and continues until electron degeneracy is removed. Then nuclear burning proceeds quietly. The maximum initial mass of the star for this to occur is  $M_{HeF}$ . Stars more massive than  $M_{HeF}$  are classified as intermediate-mass or massive depending on the physics of carbon ignition in the core. After core He-exhaustion, intermediate mass stars develop a highly degenerate CO core, and undergo helium shell flashes or thermal pulses as asymptotic giant branch (AGB) stars. The AGB phase is terminated either by envelope ejection and formation of a CO-WD (with initial mass  $M_i$  in the range  $M_{HeF} \leq M_i \leq M_w$ ) or by carbon ignition and deflagration in a highly degenerate core, once it has grown to the Chandrasekhar limit of 1.4  $M_\odot$ .

The limit mass  $M_w$  is regulated by the efficiency of mass loss by stellar wind during the RGB and AGB phases. The minimum mass of the CO core, below which carbon ignition in non degenerate condition fails and the above scheme holds, is 1.06  $M_\odot$ . The initial mass to reach a core of 1.06  $M_\odot$  is called  $M_{up}$ . The exact value of  $M_{HeF}$ ,  $M_{up}$ , and  $M_w$  depends on many details of stellar physics.  $M_w$  is mainly controlled by mass loss during the AGB phase and is about 6  $M_\odot$ . The values of  $M_{HeF}$  and  $M_{up}$  are  $\simeq 1.8 - 2.2M_\odot$  and  $\simeq 7 - 9M_\odot$ , respectively, in absence of convective overshooting. These ranges become  $M_{HeF} \simeq 1.7 - 1.8M_\odot$  and  $M_{up} \simeq 6M_\odot$  when convective overshooting is included (Chiosi et al. 1992). Since the ignition mass for a fully degenerate fully relativistic CO core is 1.46  $M_\odot$ , the possibility that C-ignition may occur in single CO-WDs is definitely ruled out.

### 2.2 Physical state of WD interiors

**Generalities.** The interiors of CO-WDs are made of ions of C, O, traces of other elements, and free electrons. Ions are fully ionized and electrons form a uniform background. In other words, there is a multi-component mixture (customarily named multi-component plasma, MCP) of ion species  $i = 1, 2, \dots$  with mass numbers  $A_i$ , atomic number  $Z_i$ , and number densities  $n_i$ . The total number density is  $n = \sum_i n_i$ . For one component plasma (OCP) the suffix  $i$  is omitted. A two components medium is defined a binary ionic medium or BIM.

The number density is related to the mass density  $\rho$  of the matter by

$$n_i = \frac{X_i \rho}{A_i m_u} \quad (1)$$

where  $X_i$  is the mass fraction or abundance of ions  $i$ , and  $m_u$

the atomic mass unit ( $m_u = 1.660 \times 10^{-24} g$ ). If the density is not very high, the total mass fraction contained in the nuclei is  $X_N = \sum_i X_i \approx 1$ , whereas for a density higher than  $\sim 4 \times 10^{11} g cm^{-3}$  above which neutrons may be free,  $X_N < 1$ . Introducing the fractional number  $x_i = n_i/n$ , with  $\sum_i x_i = 1$ , we use two groups of useful relationships:

$$\langle Z \rangle = \sum_i x_i Z_i, \quad \langle A \rangle = \sum_i x_i A_i \quad (2)$$

where  $\langle Z \rangle$   $\langle A \rangle$  are the mean atomic and mass number of ions and

$$n_e = n \langle Z \rangle, \quad \rho = \frac{m_u n \langle A \rangle}{X_N}, \quad x_i = \frac{X_i / A_i}{\sum_j X_j / A_j}. \quad (3)$$

The physical state is best described by the Coulomb coupling parameter  $\Gamma_i$  for ions  $i$ :

$$\Gamma_i = \frac{(Z_i e)^2}{a_i k_B T} = \frac{Z_i^2 e^{5/3}}{a_e k_B T} \quad (4)$$

$$a_e = \left[ \frac{3}{4\pi n_e} \right]^{1/3}, \quad a_i = Z_i^{1/3} a_e, \quad a_i = \left[ \frac{3}{4\pi n_i} \right]^{1/3} \quad (5)$$

where  $T$  is the temperature,  $k_B$  the Boltzmann constant,  $a_e$  the electron-sphere radius, and  $a_i$  the ion -sphere radius (a radius of a sphere around a given ion, where the electron and ion charge balance each other). The coupling parameter  $\Gamma_i$  is the ratio between the Coulomb energy,  $E_C = \frac{(Z_i e)^2}{a_i}$ , to the thermal energy  $E_{th} = k_B T$  of the ions. If  $\Gamma_i \ll 1$  the ions constitute an almost ideal Boltzmann gas. If  $\Gamma_i \geq 1$  the ions are strongly coupled by the Coulomb forces and constitute a Coulomb liquid or a solid. The transition gas to liquid occurs smoothly at  $\Gamma_i \sim 1$  with no phase transition. According to Lindemann (1910) and recent accurate Monte Carlo simulations by Dewitt et al. (2001), a classical OCP of ions solidifies at  $\Gamma_i \simeq 175$  via a weak second-order phase transition.

In most cases, BIMs or MCPs are supposed to represent the composition of WDs, therefore it may be useful to introduce the mean ion Coulombian parameter  $\langle \Gamma \rangle = \sum_j x_j \Gamma_j$ . Strongly coupling occurs if  $\langle \Gamma \rangle \geq 1$ , causing a transition from plasma to liquid. The temperature  $T^L$  at which this occurs is given by

$$k_B T^L = \sum_j \left[ \frac{Z_j^2 e^2}{a_j} \right] x_j \equiv k_B T \langle \Gamma \rangle. \quad (6)$$

With decreasing temperature, the ion motions can no longer be considered as classical, but must be quantized. The nuclei form a Debye plasma with temperature  $T^P$  associated with the ion plasma frequency  $\omega^P$

$$T^P = \frac{\hbar \omega^P}{k_B}, \quad \omega^P = \sqrt{\sum_j \frac{4\pi Z_j^2 e^2 n_j}{A_j m_u}}. \quad (7)$$

This is the critical stage at which the specific heat of the material is determined by nuclei oscillations of frequency  $\omega_P$  rather than by free thermal motions.

Increasing  $\langle \Gamma \rangle$  further, by either lowering the temperature or increasing the density or both, the matter crystallizes

into a rigid Coulomb lattice. The solidification (or melting) temperature  $T^M$  is given by

$$T^M = \frac{1}{k_B} \sum_j \left[ \frac{Z_j^2 e^2}{a_j} \right] x_j = \frac{T^L}{\langle \Gamma \rangle_M} \quad (8)$$

where  $\langle \Gamma \rangle_M = 175$  (Dewitt et al. 2001). At such high densities, even the small zero point oscillation allow the neighbouring nuclear wave functions to overlap, inducing nuclear reactions that depend on density and not on temperature. This is the pycno-nuclear regime.

**WD cooling.** After a short lived initial phase, during which the energy supply is sustained by some nuclear burning in the two progressively extinguishing surface shells and the large energy losses by neutrinos emission, the evolutionary rate of the WD is driven only by the internal energy of the ions and electrons. Owing to the very different specific heat at constant volume of ions and electrons, the ions are the dominating source. While the ions cool down, the WD undergoes several phase transitions. When the temperature is  $\simeq 10^8 K$ , the WD is gaseous and the ions behave like a perfect Maxwell-Boltzmann gas. As the temperature decreases, first the ions become liquid and eventually they form a solid lattice. Because the electrons are fully degenerate, they cannot cool down.

At this stage, in the energy conservation equation  $\frac{L_r}{dM_r} = \epsilon_n + \epsilon_g + \epsilon_\nu$  (with obvious meaning of all the symbols)  $\epsilon_n$  and  $\epsilon_\nu$  can be neglected and the gravitational term  $\epsilon_g = -C_v \dot{T} + \frac{\partial}{\partial \rho} \left( \frac{\partial L}{\partial T} \right)_\nu \dot{\rho}$  is approximated as  $\epsilon_g \simeq -C_v \dot{T}$ . Therefore the luminosity of a WD is given by

$$L = - \int_0^M C_v \dot{T} dM_r \quad (9)$$

where  $C_v$  and  $\dot{T}$  are function of the position and time.

As the interior of a WD cools down, the ion specific heat  $C_v^{ion}$  per gram gradually changes from

$$C_v^{ion} \simeq \frac{3}{2} \frac{k_B}{Am_u} \quad \text{to} \quad C_v^{ion} \simeq 3 \frac{k_B}{Am_u}$$

(with the usual meaning of all the symbols) whereby the first relation is for the hot gaseous phase and the second one is for the phase in which the temperature has decreased but it is still far from the Debye value (whereby quantum effects become important). The increase by a factor of 2 is due to increasing correlations of the ion positions driven by the growing importance of the Coulomb interaction energies as compared to the thermal energies of the ions. In other words, the spatial scale of the coulombian interactions is comparable to the inter-ion spacing determined by the density. When the temperature is close to the Debye value,  $C_v^{ion}$  decreases dramatically and becomes proportional to  $T^3$ .

As far as electrons are concerned, the specific heat of the electrons can be neglected with respect to that of ions and their contribution to the cooling rate of the WD can be ignored (Kippenhahn & Weigert 1990). To conclude, as the ions are the main contributors to the luminosity of a WD, the above relationships are used to calculate the cooling sequence of a WD (see Section 3.5 below).

**Liquefaction and crystallization.** The liquefaction and crystallization theory (van Horn 1968) predicts that in

WDs ions start to liquefy and freeze in an ordered crystalline lattice from the center to the outer layers when the temperature falls below  $T^L$  and  $T^M$ . The phase transition from an isotropic Coulomb liquid to a crystalline solid implies a discontinuity in the distribution of the plasma ions. Because symmetry cannot be achieved instantaneously, the transition is a first-order phase change. Therefore, for  $\langle \Gamma \rangle = \langle \Gamma \rangle_m = 172 - 175$  (Kitamura 2000) latent heat is released (van Horn 1968).

For a ionic mixture with more than one species of ions, chemical separation may occur, either at solidification or in the fluid phase. The mixture behaviour, in this case, derives from the peculiar shape of the state diagram. Because a phase separation, with the companion stratification of elements, is a source of gravitational energy (caused by sinking of the heavier ions), able to deeply modify the WD cooling time, it is of fundamental importance to obtain detailed phase diagrams for the BIM or MCP of interest. Moreover, for an accreting WD, chemical separation may produce chemical stratification, thus affecting the electron capture, opacity and fusion rates.

The most difficult problem with a strongly coupled MCP at low temperatures is understanding its actual state. MonteCarlo simulations of the freezing of classical OCP by DeWitt et al. (1992) indicate that it freezes into imperfect body-centered cubic (BCC) or faced-centered cubic (FCC) micro-crystals. Unfortunately there are no reliable simulations of freezing for MCPs. Cold MCPs are much more complex than OCPs; they can be regular lattices with impurities or an amorphous uniformly mixed structure or a lattice of one phase with admixtures of other ions; or even a mosaic of phase separated regions. Fortunately, these extreme conditions are seldom reached. In a typical CO-WD (with  $X_C = X_O = 0.5$ ), the temperature and density plane is confined in the ranges  $7.5 \leq \log \rho \leq 10.5$  and  $7.0 \leq \log T \leq 9.5$ . At  $\rho > 4 \times 10^{10} \text{ g cm}^{-3}$  the carbon nuclei cannot survive in dense matter because of beta captures. At  $\rho > 2 \times 10^{10} \text{ g cm}^{-3}$ , the oxygen nuclei are also destroyed by beta captures. In this plane, the loci of  $T^L$ ,  $T^P$  and  $T^M$  are straight lines whose terminal points  $[\log \rho, \log T]$  are:  $T^L[8.4, 9.5]$ ,  $T^P[10.5, 8.8]$ , and  $T^M[10.5, 7.9]$ . There is some marginal effect that depends on the fractional abundances  $x_j$  (see Yakovlev et al. 2006, for more details).

### 2.3 Current models of WDs

Because in first approximation, the EOS of WDs does not depend on the temperature but only on the density, the polytropic description can be used, i.e. the mechanical and thermal structure of the WDs can be treated separately (Chandrasekhar 1939). However, whenever the thermal history of a WD is required to estimate correctly the nuclear energy release or the luminosity as a function of time, or other details of the cooling sequence, complete models of WDs are required. Both types of models have been calculated by many authors and have been made available in the literature. To mention a few, recent state-of-the-art models of WDs have been calculated by Althaus & Benvenuto (1997, 1998), Althaus et al. (2009, 2012, 2013), Miller Bertolami et al. (2013), Panei et al. (2007), Renedo et al. (2010), and Salaris et al. (2010, 2013). Such models will be used in our analysis.

**Table 1.** Masses  $M_G$  (in units of  $M_\odot$ ) and radii  $R$  (in units of  $R_\odot$ ) of CO WDs at varying the central density  $\rho_c$  (in  $\text{g cm}^{-3}$ ). The mass is the gravitational mass; it tends to the Chandrasekhar limit as the density goes to infinity.

$\log \rho_c$	$M_G$	$R$	$\log \rho_c$	$M_G$	$R$
5.29	0.20	$2.10 \times 10^{-2}$	8.29	1.24	$5.33 \times 10^{-3}$
5.57	0.27	$1.87 \times 10^{-2}$	8.57	1.30	$4.54 \times 10^{-3}$
5.71	0.31	$1.77 \times 10^{-2}$	8.71	1.32	$4.19 \times 10^{-3}$
5.85	0.35	$1.67 \times 10^{-2}$	8.85	1.34	$3.85 \times 10^{-3}$
6.00	0.40	$1.57 \times 10^{-2}$	9.00	1.36	$3.54 \times 10^{-3}$
6.29	0.51	$1.39 \times 10^{-2}$	9.29	1.38	$2.98 \times 10^{-3}$
6.57	0.63	$1.23 \times 10^{-2}$	9.57	1.40	$2.49 \times 10^{-3}$
6.71	0.69	$1.16 \times 10^{-2}$	9.71	1.41	$2.27 \times 10^{-3}$
6.85	0.75	$1.08 \times 10^{-2}$	9.85	1.41	$2.07 \times 10^{-3}$
7.00	0.81	$1.02 \times 10^{-2}$	10.00	1.42	$1.88 \times 10^{-3}$
7.29	0.93	$8.89 \times 10^{-3}$	10.29	1.42	$1.55 \times 10^{-3}$
7.57	1.04	$7.73 \times 10^{-3}$	10.57	1.42	$1.28 \times 10^{-3}$
7.71	1.09	$7.20 \times 10^{-3}$	10.71	1.42	$1.15 \times 10^{-3}$
7.85	1.14	$6.69 \times 10^{-3}$	10.85	1.42	$1.04 \times 10^{-3}$
8.00	1.18	$6.21 \times 10^{-3}$	11.00	1.42	$9.44 \times 10^{-4}$

**Table 2.** Properties of the progenitor star at the start of the TP-AGB phase prior to the formation of the WD.  $M_i$ ,  $M_{CO}$ ,  $M_{WD}$  are in  $M_\odot$ ,  $\rho_c$  is in  $\text{g cm}^{-3}$ , the age is in years.  $M_{WD}$  is derived from eqn. (10).  $\rho_c$  is interpolated from Table 1.

$M_i$	Y=0.26	Z=0.017	$\log \rho_c$	$Age(yr)$
	$M_{CO}$	$M_{WD}$		
6.0	0.956	1.14	7.95	$7.881 \times 10^7$
5.0	0.869	1.04	7.60	$1.233 \times 10^8$
4.0	0.802	0.87	7.15	$2.216 \times 10^8$
3.0	0.725	0.75	6.84	$4.999 \times 10^8$
2.0	0.625	0.64	6.56	$1.464 \times 10^9$
1.0	0.524	0.53	6.35	$1.269 \times 10^{10}$
0.8	0.517	0.52	6.25	$2.899 \times 10^{10}$

In concluding this section, we need to present and shortly discuss a few relationships between important parameters of WDs such as (i) the initial mass  $M_i$  of the progenitor star, (ii) the CO core mass,  $M_{CO}$ , at the beginning of the TP-AGB phase, (iii) the central density and the age of the progenitor at the end of the AGB phase, (iv) the mass  $M_{WD}$  of the descendent WD (which is also named the gravitational mass  $M_G \equiv M_{WD}$ ), and finally (v) the central density, radius, and age.

A recent empirical estimate of the relationship between  $M_{WD}$  and  $M_i$  has been given by Catalán et al. (2008) to whom we refer whenever necessary

$$\begin{aligned}
 M_{WD} &= (0.096 \pm 0.005)M_i + (0.429 \pm 0.015) \\
 &\quad \text{for } M_i < 2.7M_\odot \\
 M_{WD} &= (0.137 \pm 0.007)M_i + (0.318 \pm 0.018) \\
 &\quad \text{for } M_i > 2.7M_\odot. \quad (10)
 \end{aligned}$$

The relationships between the central density  $\rho_c$ , the mass  $M_G \equiv M_{WD}$ , and the total radius are derived from Althaus & Benvenuto (1997, 1998) and are reported in Table 1. The cooling sequences for the same WD masses are also from Althaus & Benvenuto (1997, 1998). The mass

$M_{CO}$  of the CO core at the beginning of the TP-AGB phase and the age of the progenitor are from the Padova Library of stellar models (Bertelli et al. 2008, 2009) and are listed in Table 2. Owing to the very short duration of the TP-AGB phase, the stellar age at the beginning of this phase nearly coincide with the age of the progenitor star when the CO core is exposed and the WD phase begins. We neglect here the effects of the initial chemical composition on  $M_{CO}$ ,  $M_{WD}$  and ages, and focus on the case  $[Y=0.26, Z=0.017]$  typical of a young population. If the chemical composition is taken into account, because of the different total lifetimes of stars of the same mass but different chemical composition and other details of stellar structure, at the low mass end of the WD mass distribution not all combinations of  $M_i$  and  $M_{WD}$  correspond to realistic cases. The lower mass limit is determined by the age of the Universe, i.e.  $13.7 \pm 0.2$  Gyr according to WMAP data (Spergel et al. 2003).

Finally, we would like to remind that, owing to the different mass size of the external envelope surrounding the  $M_{CO}$  core of TP-AGB stars, the core increases little during this phase in low mass stars (up to about  $3M_\odot$ ) while it increases significantly in stars with mass in the range  $3M_\odot$  to  $6M_\odot$ . Furthermore, the upper mass limit  $M_{up}$  for AGB phase to occur (and to WDs to be generated) depends on the initial chemical composition; the detailed stellar models by Bertelli et al. (2008, 2009) show that it can vary from  $5M_\odot$  to  $6M_\odot$ . Therefore the  $M_{WD}$  vs  $M_i$  relationship of Table 2 has to be considered as only indicative of the overall trend.

### 3 NUCLEAR BURNING IN WDS

#### 3.1 Generalities

In the first stages of the WD life, nuclear burning can occur in two shells, close to the surface (see Renedo et al. 2010; Córscico & Althaus 2014, and references therein). Hydrogen may still be burning via the CNO-cycle, because a small amount of it (mass abundances in the range  $10^{-4} \leq X_H \leq 10^{-5}$ ) is left on the surface, and the temperature is still sufficiently high to sustain nuclear burning. Similarly, somewhat deeper inside there may be also residual He-burning in a shell surrounding the inert CO-core.

In general, as the temperature decreases, all thermal nuclear burnings are turned off for billions of years until the WD has cooled down to very low temperature, so that the pycno-nuclear regime is reached. This is possible only when the internal energy of ions and the WD luminosity are very low, and the baryonic matter (mostly C and O ions) is crystallized, usually when the WDs are quite old (several Gyrs). An exception to the above picture are the results of Miller Bertolami et al. (2013) who have recently shown that for low-mass WDs resulting from low-metallicity progenitors, residual H-burning constitutes the main contributor to the stellar luminosities for luminosities as low as  $\log L/L_\odot \simeq -3.2$ .

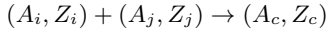
The pycno-nuclear reactions were studied long ago by Salpeter & van Horn (1969). These authors modeled the pycno-nuclear potential with a harmonic oscillator and discussed the possible influence of electron-screening and other effects. They also suggested that impurities may significantly

increase the nuclear burning rates (see Section 4). This suggestion is the starting point of this study.

Other formulations of nuclear reactions in the pycno-nuclear regime are by Schramm & Koonin (1990), Ogata et al. (1991), Ichimaru et al. (1992), Kitamura & Ichimaru (1995), Brown & Sawyer (1997), Ichimaru & Kitamura (1999a), Kitamura (2000), Gasques et al. (2005), Yakovlev et al. (2006), Beard (2010), and references therein. All these authors considered and derived the pycno-nuclear reaction rates for a lattice composed of a single element (the one-component plasma OCP of Gasques et al. 2005), two elements (the binary ionic medium BIM of Kitamura 2000), or a multi-component plasma (MCP) of (Yakovlev et al. 2006). They also discussed electron screening and phase transitions from gaseous to liquid to solid phases. However, they did not discuss the presence of impurities (see Section 3.5).

### 3.2 Formalism for reaction rates

We are interested in nuclear fusion reactions



where  $A_c = A_i + A_j$ ,  $Z_c = Z_i + Z_j$  refer to the compound nucleus  $c$ . To study these reactions we must extend the formalism presented in Sect. 2.2 and introduce the ion-sphere quantities

$$a_{ij} = \frac{a_i + a_j}{2}, \quad \mu_{ij} = m_u \frac{A_i A_j}{A_c}, \quad \Gamma_{ij} = \frac{Z_i Z_j e^2}{a_{ij} k_B T} \quad (11)$$

$$\begin{aligned} T_{ij}^L &= \frac{Z_i Z_j e^2}{a_{ij} k_B} \\ T_{ij}^P &= \frac{\hbar}{k_B} \omega_{ij} \quad \omega_{ij}^P = \sqrt{\frac{4\pi Z_i Z_j e^2 n_{ij}}{2\mu_{ij}}} \\ T_{ij}^M &= \frac{Z_i Z_j e^2}{a_{ij} \Gamma_{ij}^M} \end{aligned} \quad (12)$$

where  $\mu_{ij}$  is the reduced mass,  $a_{ij}$  characterizes the equilibrium distance between neighbouring nuclei (the corresponding number density is  $n_{ij} = 3/4\pi a_{ij}^3$ ),  $\Gamma_{ij}$  describes their coulomb coupling,  $T_{ij}^L$  is the temperature of the onset of strong coupling (or liquefaction temperature),  $T_{ij}^P$  is the Debye temperature for the oscillations of ions  $i$  and  $j$ , and  $T_{ij}^M$  is the melting or solidification temperature<sup>1</sup>. Finally, we need the generalized Bohr radius

$$r_{Bij} = \frac{\hbar^2}{2\mu_{ij} Z_i Z_j e^2} \quad (13)$$

which becomes the ion Bohr radius for equal ions  $i = j$ , and the parameter  $\lambda_{ij}$ , corresponding to the parameter  $\lambda$  introduced by Salpeter & van Horn (1969)

$$\lambda_{ij} = r_{Bij} \left(\frac{n_{ij}}{2}\right)^{1/3} = \frac{2r_{Bij}}{(Z_i^{1/3} + Z_j^{1/3})} \left(\frac{\rho X_N \langle Z \rangle}{2\langle A \rangle m_u}\right)^{1/3} \quad (14)$$

<sup>1</sup> In the case of an OCP all the symbols reduce to those already defined in Sect. 2.2

### 3.3 Five regimes of nuclear burning

In WDs the central density ranges from  $10^6 \text{ g cm}^{-3}$  to  $10^{10} \text{ g cm}^{-3}$  depending on the initial mass of the star, and the density decreases from the center to the surface, so we must consider a wide range of densities. The temperature also spans a wide range, from  $10^8 \text{ K}$  at the beginning of the cooling sequence to typical values of about  $10^5 \text{ K}$  after a few Gyrs. In the plane  $T - \rho$ , the WD undergoes two phase transitions: from gas to liquid and from liquid to solid (crystallization). In parallel to this, there are five burning regimes (see Salpeter & van Horn 1969; Yakovlev et al. 2006; Beard 2010): (i) the classical thermo-nuclear; (ii) the thermo-nuclear with strong electron screening; (iii) the thermo-pycno-nuclear; (iv) the thermally enhanced pycno-nuclear; (v) and eventually the zero temperature pycno-nuclear. For a complete description of the regimes see Beard (2010). The five regimes have the following characteristics:

i) The classical thermo-nuclear one takes place when  $\Gamma_{ij} \ll 1$ . The mean inter-nuclear distance is much greater than the typical scale at which the particles feel electrostatic interaction: the nuclei are fully stripped and there is a small screening effect from the background electron gas. The bulk matter behaves like an ideal gas.

ii) The second regime is bounded by the temperatures  $T_{ij}^L$  and  $T_{ij}^P$  with  $T_{ij}^P \leq T \leq T_{ij}^L$ . For temperatures lower than  $T_{ij}^L$  the ions are in the liquid phase, and for temperatures close to  $T_{ij}^P$ , the ions cannot be considered a free gas but part of a lattice with vibrations  $\omega_{ij}^P$ . The thermonuclear burning associated to very strong electron screening operates in this temperature range.

iii) The third regime corresponds to the temperature range  $T_{ij}^M \leq T \leq T_{ij}^P$  and  $\Gamma_{ij} \geq 1$ . Nuclei are bound to the lattice sites, so that the reactions occur between highly thermally excited bound nuclei, which oscillate with frequencies higher than the plasma frequency and have energy greater than the zero point energy of the plasma. The nuclei are also embedded in a highly degenerate electron gas, so that the reaction rates are enhanced by the charge screening electron background. For  $\Gamma_{ij}^M \geq 175$ , and temperatures lower than  $T_{ij}^M$ , the nuclei form a solid lattice.

iv) In the thermally enhanced pycno-nuclear regime,  $\Gamma_{ij} \gg 1$  but the melting temperature is not yet reached (this requires  $\Gamma_{ij} \geq 175$ ). Most of the nuclei are bound to the lattice, but some nuclei are highly excited states, and reactions may occur between neighboring pairs of these nuclei. Electron screening is always very strong.

v) The last domain is the one of pure pycno-nuclear behaviour ( $T \simeq 0$ ). Almost all the ions are in the fundamental state of the lattice (now crystallized to a solid) but their energies are larger than zero because of the Heisenberg indeterminacy principle. Therefore, there is still a finite possibility of penetrating the Coulomb barrier (tunneling effect). Reactions are possible only between closest pairs. Because there is no longer a temperature dependence, these reactions are referred to as  $T = 0$  pycno-nuclear rates.

### 3.4 Thermal vs pycno-nuclear burnings

There are some important differences in the hypotheses underlying thermo-nuclear and pycno-nuclear reactions that are worth highlighting. In the thermo-nuclear reactions each

particle can interact with all the others, therefore the rate contains the product of the two densities of the two interacting species. The reaction rate is

$$R_{ij} = N_i N_j \langle \sigma v \rangle \quad (15)$$

The probability of interaction is proportional to the product of two factors: the Maxwell-Boltzmann statistical factor and the probability of tunneling. Their product gives origin to the so-called Gamow window. The first factor is proportional to

$$e^{-E/(k_B T)} \quad (16)$$

whereas the second one is proportional to

$$e^{-\sqrt{E_G/E}} \quad (17)$$

where  $E_G$  is the Gamow energy. If we define  $E_{ij}^{pk} = \frac{1}{2}\sqrt{E_G k_B T}$  we can write the thermo-nuclear reaction rate as

$$R_{ij}^{th} = 4 \frac{n_i n_j}{1 + \delta_{ij}} \left( \frac{2E_{ij}^{pk}}{3\mu_{ij}} \right)^{1/2} \frac{S(E^{pk})}{k_B T} e^{-\tau_{ij}} \quad (18)$$

with  $\tau_{ij} = \frac{3E_{ij}^{pk}}{k_B T}$ .

The rate for the pycno-nuclear reactions is quite different. Each nucleus in the lattice can interact only with the nearest neighbours. Therefore, the rate is

$$R_i^{pyc} = \frac{n_i}{2} \langle \nu_i p_i \rangle \quad (19)$$

where  $p_i$  is the reaction probability between a pair of ions and  $\nu_i$  is the number of nearest neighbours. According to Salpeter & van Horn (1969), the reaction rate probability can be written as

$$p_i = D_{pyc} \frac{\lambda_i^{3-C_{pl}} S(E_i^{pk})}{\hbar r_{Bi}^2} \exp\left(\frac{-C_{exp}}{\lambda_i^{1/2}}\right) \quad (20)$$

where  $\lambda_i$  is the ratio of the Bohr radius to the lattice spacing. For more details on the meaning of the various symbols see Salpeter & van Horn (1969); Beard (2010) and Shapiro & Teukolsky (1983).

### 3.5 Rates for pycno-nuclear reactions in mono- and multi-component fluids

In the literature on pycno-nuclear reactions, there are basically three different formulations or models: (i) the classical one, based on the simple harmonic oscillator at zero temperature proposed long ago by Salpeter & van Horn (1969), that we will shortly revisit to explore the effect of impurities (Sect. 4), (ii) the model by Kitamura (2000, and references) and finally (iii) the models by Gasques et al. (2005) and Yakovlev et al. (2006). The last two models include also the effect of temperature, and they are mutually consistent although they make use of different analytical expressions.

#### 3.5.1 Summary of the Kitamura (2000) reaction rates

Kitamura (2000, see also references therein) considerably improved the simple description based on the harmonic oscillator. He derived analytic expressions for the reaction rates, taking into account the dielectric functions of relativistic and non-relativistic electrons, the screening potentials based on the Monte Carlo simulations, and the interaction free energies in dense electron screened BIMs. He found that under-barrier reaction rates can be expressed as the product of three terms

$$R = R_G A_{ij}^{(0)} A_{ij}^{(e)} \quad (21)$$

where  $R_G$  is the so-called Gamow channel, representing the basic binary interaction between any two particles, and is expressed as the Gamow rate. It is dominant in tenuous plasmas in which the effect of surrounding particles is negligible, so the nuclei interact via the bare Coulomb potential and the rate is expected to be strongly dependent on temperature. The other two terms take the effects of the surrounding particles into account. The so-called few-particles interactions are expressed by  $A_{ij}^{(0)}$  and occur independently of the aggregation state of nuclei. The shielding effect stems from local variations of particle density with respect to the background (also referred to as polarization). The net effect is to reduce the Coulomb potential barrier and to strongly enhance the rate. Once the temperature is below a certain value, the rate is expected to increase as the temperature decreases. Finally the third term  $A_{ij}^{(e)}$  is due to the many-particles processes that may occur when the electrons can be considered as a uniform background. This is expected to produce a small effect at the typical temperatures and densities of liquid-solid WDs, because the so-called screening temperature  $T_s$ , at which this effect is important, is much lower. Therefore, the third term is expected to be small and to become dominant only at very low temperatures, unlikely to be reached in WDs.

The most important pycno-nuclear reactions are the few-particles ones rather than the many-particles interactions. Quoting Ichimaru & Kitamura (1999b, page 2694) "Since the enhancement factors generally increase steeply with lowering of the temperature, a maximum pycno-nuclear rate may be attained in a liquid-metallic substance near the conditions of freezing transitions; reaction rates in a solid, depending on the amplitudes of atomic vibrations, increase with the temperature".

Kitamura (2000)'s rates are particularly useful to understand the effects of impurities because they include both BIMs and OCPs, and provide a better description of the physics during the solid transition, which implies a smoother discontinuity in the reaction rates. We will apply the Kitamura (2000) rates over the whole range of temperatures and densities, for any kind of reacting pairs.

In a BIM of two elements "i" and "j", with charges  $Z_i$  and  $Z_j$ , mass number  $A_i$  and  $A_j$ , mass fraction  $\rho_m$  and temperature  $T$ , the reaction rates are

$$R_{ij}(\text{reactions cm}^{-3} \text{ s}^{-1}) = \frac{1}{1 + \delta_{ij}} \frac{X_i X_j (A_i + A_j)}{Z_i Z_j (A_i A_j)^2} \cdot [\rho_m (\text{g cm}^{-3})]^2 \cdot [S_{ij}(E_{\text{eff}}) (\text{MeV barns})] R_0 \quad (22)$$

where  $\delta_{ij}$  is the Kröner delta function ( $\delta_{ij} = 1$  if  $i = j$  and  $\delta_{ij} = 0$  otherwise),  $S_{ij}$  is the nuclear cross-section factor for the analyzed reaction and  $R_0$  depends the aggregation state of the matter.

For the liquid phase, if  $T_s$  is the critical screening temperature and  $T \geq T_s$ , we have

$$R_0^{\text{fluid}} = 2.613 \times 10^{32} \tau_{ij}^2 \sqrt{1 - \left[ \tanh\left(\frac{T_s}{T}\right) \right]^8}^{1/12} \cdot \exp\left(-\alpha_{ij} \pi \sqrt{\frac{D_s}{r_{ij}^*}} + \xi_{ij}\right) \quad (23a)$$

if instead  $T < T_s$

$$R_0^{\text{fluid}} = 1.600 \times 10^{33} \left(\frac{D_s}{r_{ij}^*}\right)^{1/2} \left\{ 1 + \left[ 0, 543 \left(\frac{D_s}{r_{ij}^*}\right)^{1/2} - 1 \right] \cdot \left(\frac{T}{T_s}\right)^3 \right\} \exp\left(-\alpha_{ij} \pi \sqrt{\frac{D_s}{r_{ij}^*}} + \xi_{ij}\right) \quad (23b)$$

where  $T_s$  is the critical screening temperature at which the Gamow peak energy equals the electrostatic screening energy. The two expressions coincide for  $T = T_s$ .

The nuclear reaction rates for the solid state are obtained by substituting in eqn.(22), the following expression for  $R_0$ :

$$R_0^{\text{solid}} = 4.83 \cdot 10^{32} (R_s^{ij})^{1.809} \cdot \exp\left\{ \left[ -3.506 + 0.142 \left(\frac{a_{ij}}{D_s}\right) + 0.144 \left(\frac{a_{ij}}{D_s}\right)^2 + F(Y_{ij}^s) \right] (R_s^{ij})^{1/2} \right\}. \quad (24)$$

The definition of all terms and meaning of all symbols used in eqns. (23) and (24) above can be found in Kitamura (2000) to whom the reader should refer. We note that the first term in the exponential factor of eqns. (23) corresponds to the Gamow thermo-nuclear channel, while the second term corresponds to the under-barrier reaction channel. In this paper, we examine the reactions listed in Table 4. The experimental value of the cross-section factor and  $Q$ -value from Fowler et al. (1975) are also in Table 4.

### 3.5.2 Summary of the Gasques - Yakovlev reaction rates

Gasques et al. (2005) elaborated a model for OCPs to calculate the reaction rates in several regimes, from thermo-nuclear to pycno-nuclear. Subsequently Yakovlev et al. (2006) and Beard (2010) extended the model to MCPs. These three papers are based on the Sao Paulo potential, that takes into account the effect of Fermi statistic on the

nucleons of the interacting nuclei. The purposes of these studies are: (a) to evaluate the rate for the pycno-nuclear part  $R_{ij}^{\text{pyc}}$  and (b) to apply a phenomenological expression for the temperature and density dependent part  $\Delta R_{ij}(\rho, T)$ . All the auxiliary quantities contained in the expressions below have already been introduced in Sect. 2.2 or are given in Table 3.

The pycno-nuclear component is

$$R_{ij}^{\text{pyc}} = 10^{46} C_{\text{pyc}} \frac{8\rho X_N x_i x_j A_i A_j \langle A \rangle Z_i^2 Z_j^2}{(1 + \delta_{ij}) A_c^2} S(E_{ij}^{\text{pk}}) \times \tilde{\lambda}_{ij}^{3-C_{pl}} \exp\left(-\frac{C_{\text{exp}}}{(\tilde{\lambda}_{ij})^{1/2}}\right) \text{cm}^{-3} \text{s}^{-1} \quad (25)$$

whereas the phenomenological expression for the temperature and density dependent part of the rate that combines all the burning regimes is

$$R_{ij}(\rho, T) = R_{ij}^{\text{pyc}}(\rho) + \Delta R_{ij}(\rho, T), \quad (26)$$

$$\Delta R_{ij}(\rho, T) = \frac{n_i n_j}{1 + \delta_{ij}} \frac{S(E_{ij}^{\text{pk}})}{\hbar} r_{Bij} P F, \quad (27)$$

$$F = \exp(-\tilde{\tau}_{ij} + C_{sc} \tilde{\Gamma}_{ij} \phi e^{-\Lambda T_{ij}^{(p)}/T} - \Lambda \frac{\tilde{T}_{ij}^{(p)}}{T}), \quad (28)$$

$$P = \frac{8\pi^{1/3}}{\sqrt{3} 2^{1/3}} \left(\frac{E_{ij}^a}{k_B T}\right)^\gamma$$

where

$$E_{ij}^a = 2\mu_{ij} Z_i^2 Z_j^2 e^4 / \hbar^2 \quad (29)$$

$$\phi = \sqrt{\Gamma_{ij}} / [(C_{ij}^{sc} / \zeta_{ij})^4 + \Gamma_{ij}^2]^{1/4} \quad (30)$$

$$\tilde{\tau}_{ij} = 3\left(\frac{\pi}{2}\right)^{2/3} \left(\frac{E_{ij}^a}{k_B T}\right)^{1/3}$$

$$\tilde{\Gamma}_{ij} = \frac{Z_i Z_j e^2}{a_{ij} k_B T}, \tilde{T} = \sqrt{T^2 + C_T^2 (T_{ij}^{(p)})^2}, \quad (31)$$

$$\gamma = (T^2 \gamma_1 + (\tilde{T}_{ij}^{(p)})^2 \gamma_2) / (T^2 + (\tilde{T}_{ij}^{(p)})^2) \quad (32)$$

$$E_{ij}^{\text{pk}} = \hbar \tilde{\omega}_{ij}^{(p)} + \left(\frac{Z_i Z_j e^2}{a_{ij}} + \frac{k_b T \tau_{ij}}{3}\right) \exp\left(-\frac{\Lambda \tilde{T}_{ij}^{(p)}}{T}\right) \quad (33)$$

where  $\gamma_1 = 2/3$  and  $\gamma_2 = (2/3)(C_{pl} + 0.5)$ . For all other details see Yakovlev et al. (2006) and Beard (2010).

### 3.5.3 Comparing the two sets of reaction rates

The rates predicted by Kitamura (2000, dashed lines) and Gasques et al. (2005, solid and dotted lines) for the  $^{12}\text{C} + ^{12}\text{C}$  reaction are shown as a function of density in Fig. 1. For the Gasques et al. (2005) rate we adopt the numerical coefficients for MCPs that are listed in Table 3 and show the cases of maximum (solid lines) and minimum (dotted lines) rates. For each case we show separately the sole pycno-nuclear component (red lines) and the pycno-nuclear plus thermal channel (blue lines). The rates by Kitamura (2000) fall always in between those by Gasques et al. (2005) for all regimes. In general, the three cases have a very similar trend, the only difference being the density at which the transition from thermal+pycno to pycno-nuclear regimes occurs and the absolute value of the rates. However, we note that



**Table 3.** Coefficients in the interpolation expressions for a reaction rate for the optimal model of nuclear burning and for the models which maximize and minimize the rate. The parameters CT,  $\alpha_{\lambda ij}$ ,  $\alpha_{\omega ij}$  are different for the multi-component plasma (MCP) and one component plasma (OCP) (the values for OCP are given in brackets). For a MCP, the models assume a uniformly mixed state (see Yakovlev et al. (2006) for details).

Model	Cexp	Cpyc	Cpl	CT	$\alpha_{\lambda ij}$	$\alpha_{\omega ij}$	$\Lambda$
Optimal	2.638	3.90	1.25	0.724 (0.724)	1.00 (1)	1.00 (1)	0.5
Maximum rate	2.450	50	1.25	0.840 (0.904)	1.05 (1)	0.95 (1)	0.35
Minimum rate	2.650	0.5	1.25	0.768 (0.711)	0.95 (1)	1.05 (1)	0.65

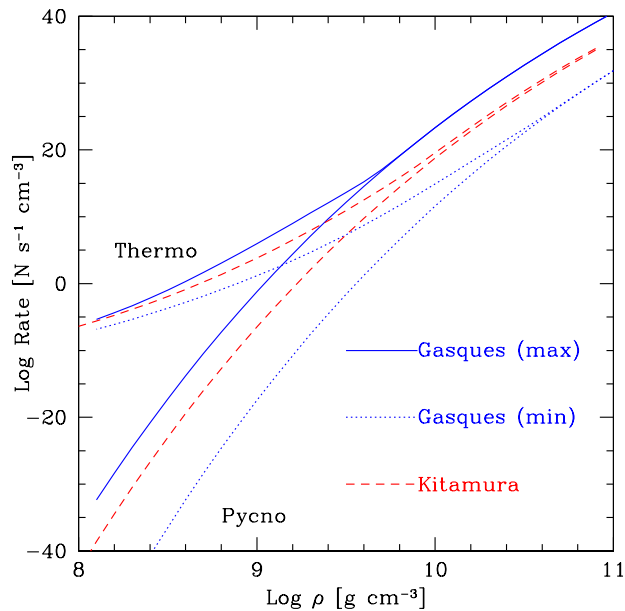


**Figure 1.** Comparison of the Gasques et al. (2005) and Kitamura (2000) rates for the  $^{12}\text{C} + ^{12}\text{C}$  reaction. The coefficients of the Gasques et al. (2005) rates are those listed in Table 3. The thermal branch and pycno-nuclear channel are calculated with temperatures of  $10^8$  K and  $10^5$  K, respectively. The mass abundance of carbon is equal to  $X_{\text{C}} = 1$ .

**Table 4.** Parameters for the reaction rates of most common reactions in CO-WDs.

Reaction	Products	Q-value [MeV]	S(0) [MeV barn]
$^{12}\text{C} + ^{12}\text{C}$	$\text{Mg}^{24}$	13.931	$8.83 \times 10^{16}$
$^{12}\text{C} + ^{16}\text{O}$	$\text{Si}^{28}$	16.754	$1.15 \times 10^{21}$
$^{16}\text{O} + ^{16}\text{O}$	$\text{S}^{32}$	16.541	$2.31 \times 10^{27}$

there is a large difference between the maximum and minimum efficiency for the Gasques et al. (2005) rates, amounting to about ten orders of magnitude, and that the Kitamura (2000) rates run closer to the Gasques et al. (2005) case with maximum efficiency. There are large differences in the rates at all densities, causing a large difference in the final results.

#### 4 IMPURITIES IN PYCNO-NUCLEAR REACTIONS RATES

When matter becomes solid, the C and O ions are in a fixed configuration in a crystal whose structure is known from solid state physics. We cannot exclude the possibility that some impurities of elements of any type are present in the lattice.

The dominant element with the lowest atomic number is carbon ( $Z_{\text{C}}=6$ ), followed by oxygen ( $Z_{\text{O}} = 8$ ), so impurities can be grouped according to their atomic number: i) heavy elements like magnesium, etc...with  $Z > Z_{\text{C}}$ ; ii) light elements like hydrogen and helium with  $Z < Z_{\text{C}}$ .

We are particularly interested here in impurities of light elements, like hydrogen and helium. In the next section, we will see that the pycno-nuclear rates for these elements may be particularly high, so the amount of light elements necessary for relevant effects is extremely low. For instance, in the case of hydrogen, abundances in the range  $10^{-16} \leq X_{\text{H}} \leq 10^{-21}$  are sufficient to produce nuclear energy in amounts comparable to the luminosity of typical WDs at suitable ages.

This should not be confused with the surface content of hydrogen that can be as high as  $X_{\text{H}} \simeq 10^{-5}$  without triggering thermo-nuclear burning (see Fujimoto 1982b,a; Renedo et al. 2010, for all details). Higher concentrations are not allowed otherwise the associated thermo-nuclear energy generation via the CNO-cycle would exceed the luminosity of a WD, probably inducing a thermonuclear runaway.

In this section we describe, with a simple formulation, how the coulombian potential and local density in a ionic lattice are modified by impurities. We adopt the expression of Salpeter & van Horn (1969) and Shapiro & Teukolsky (1983) for the rate of pycno-nuclear reactions. The original theory was developed for reactions among the same nuclei (e.g. carbon). Since we consider at least two elements (e.g. reactions among hydrogen and carbon), the columbian potential must be suitably modified. We are going to present a template, to which more sophisticated formulations must be compared.

##### 4.1 The modified Salpeter-Van Horn model

Using the same formalism of Shapiro & Teukolsky (1983), we consider an OCP made of a certain type of ions, e.g. either pure carbon or pure oxygen. In this framework, first we consider the one-dimensional potential of an array of ions and extend it to 3D. Suppose that the lattice is composed of ions of charge  $Z_1$ . In one cell we substitute the charge  $Z_1$  with a charge  $Z_2$  (for instance hydrogen or helium). If  $x$  is the displacement from the equilibrium position (see Fig.2)

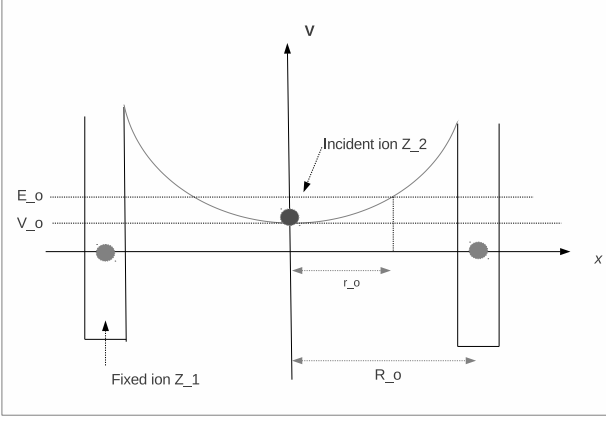


**Figure 2.** The potential governing the motion of one incident ion of charge  $Z_2$  relative to an adjacent ion of charge  $Z_1$ . Zero point energy fluctuations in the harmonic potential well near the incident ion can lead to Coulomb barrier penetration and nuclear reactions.

the coulombian potential becomes

$$V(x) = \frac{Z_1 Z_2 e^2}{R_0 - x} + \frac{Z_1 Z_2 e^2}{R_0 + x} - 2 \frac{Z_1^2 e^2}{R_0} \quad (34)$$

where  $R_0$  is the inter-ionic distance. In eqn. (34) we assume that the energy of the lattice is zero and estimate the energy variation. Removing a charge  $Z_1$  produces the negative term (interaction of the neighbouring particles with the hole) and the addition of a charge  $Z_2$  at position  $x$  introduces the positive terms. We suppose that  $x \ll R_0$  and use the Taylor expansions to derive

$$V(x) = 2 \frac{Z_1 Z_2 e^2}{R_0} - 2 \frac{Z_1^2 e^2}{R_0} + \frac{2 Z_1 Z_2 e^2 x^2}{R_0^3}. \quad (35)$$

The constant term shifts all the energy levels. The variable term

$$+ \frac{2 Z_1 Z_2 e^2 x^2}{R_0^3} \quad (36)$$

is the dominant one and behaves like a harmonic oscillator with

$$\omega = \left( \frac{4 Z_1 Z_2 e^2}{R_0^3 \mu} \right)^{1/2}. \quad (37)$$

Using the equation  $E_0 = V(r_0) = V_0 + 1/2 K r_0^2 = V_0 + 1/2 \hbar \omega$ , the turning point  $r_0$  is

$$r_0 = \left( \frac{\hbar R_0^3 / 2}{2 (Z_1 Z_2 \mu)^{1/2} e} \right)^{1/2} \quad (38)$$

The solutions of the Schrödinger equation for a harmonic oscillator are known. In three dimensions they become

$$|\psi_{SHO}|^2 = \frac{\tau^3}{\pi^{3/2}} e^{-\tau^2 r^2} \quad (39)$$

where  $\tau = 1/r_0$ . Assuming that the exponential value is one,

$$|\psi_{inc}|^2 \simeq |\psi_{SHO}|^2 \simeq \frac{1}{r_0^3 \pi^{3/2}}. \quad (40)$$

The transmission coefficient for an incident ion with energy

$E_0$  in the WKB approximation is

$$T = \exp\left[-2 \int_a^b \left( \frac{2\mu}{\hbar^2} [E_0 - V_0 - 1/2 K x^2] \right) dx\right] \quad (41)$$

where  $E_0 = V_0 + 1/2 \hbar \omega$ . Following the discussion by Shapiro & Teukolsky (1983), we obtain the reaction rate per ion pair

$$W = v |\psi_{inc}|^2 \frac{TS(E)}{E_K} \quad (42)$$

where in the limit  $r_0/R_0 \ll 1$

$$T = \frac{R_0}{r_0} \exp\left(-2 \frac{R_0^2}{r_0^2}\right). \quad (43)$$

This transmission coefficient is the leading term in the reaction rate and it strongly depends on the charge  $Z_2$ , in fact the exponent is proportional to  $(Z_1 Z_2)^{1/2}$ , which means that the transmission coefficient is much higher for  $Z_2 < Z_1$ .

We refer to our revision of the Shapiro & Teukolsky (1983) rate as the "modified harmonic oscillator" (MHO). We will later adopt the formulations of Kitamura (2000) and Yakovlev et al. (2006), but the MHO approximation is an efficient way to explore reactions between light and heavier elements when the WD reaches the pycno-nuclear regime. We note that the same formalism can be applied to the case of MCPs because what matters are the pairs of interacting ions, e.g.  $^1\text{H} + ^{12}\text{C}$  or  $^1\text{H} + ^{16}\text{O}$ . The lower coulombian barrier in the case of  $^{12}\text{C}$  and  $^1\text{H}$  definitely favours this ion pair, so most of discussion will be limited to these two elements.

## 4.2 Local densities around impurities

In order to evaluate the change in the local density and consequently in the rates of energy production by pycno-nuclear reactions caused by impurities, OCPs and MCPs must be treated separately. We can consider three cases:

(i) **OCPs, neglecting electrons in the electrostatic force.** Let us consider an array of nuclei of charge  $Z_1$  (e.g. carbon) as shown in the top panel of Fig. 5. If in one site we substitute the nucleus of charge  $Z_1$  with a nucleus of charge  $Z_2$ , e.g. hydrogen (the impurity), the carbon nuclei neighbouring the hydrogen nucleus are shifted toward it because of the new equilibrium of the forces as indicated by the arrows (the situation is clearly symmetric). The equilibrium of the forces is expressed by

$$\frac{Z_1 Z_2}{(R_0 - x)^2} = \frac{Z_1^2}{(R_0 + x)^2}. \quad (44)$$

After developing the squares we obtain

$$(Z_1 Z_2 - Z_1^2) x^2 + 2 R_0 (Z_1 Z_2 + Z_1^2) x + (Z_1 Z_2 - Z_1^2) R_0^2 = 0. \quad (45)$$

This is a second order equation with two solutions

$$x_{1,2} = R_0 \left[ - \frac{(Z_1 Z_2 + Z_1^2)}{(Z_1 Z_2 - Z_1^2)} \pm \sqrt{\left[ \frac{(Z_1 Z_2 + Z_1^2)}{(Z_1 Z_2 - Z_1^2)} \right]^2 - 1} \right]. \quad (46)$$

We evaluate the displacement for  $Z_1 = 6$  (carbon) and  $Z_2 = 1$  (hydrogen) and keep only the solution  $< 1$  that has physical meaning. We obtain  $R'_0 = R_0 - x = 0.58 R_0$ , i.e. the new local inter-ion distance  $R'_0$  is smaller than in the

unperturbed case. For the case  $Z_1 = 6$  (carbon) and  $Z_2 = 2$  (helium) obtaining  $R_0 - x = 0.73 R_0$ . As expected, the effect is decreasing with increasing  $Z_2$ . Hereinafter  $R'_0$  is renamed  $R_0$ .

**(2) OCPs with electrons in the electrostatic force.** In the above expression we neglected the contribution by electrons to the balance of electrostatic forces among ions. Taking electrons into account, we assume that in the space between the ions  $Z_1$  and  $Z_2$  electrons distribute uniformly and evaluate the field due to electrons at any distance  $x$  in between the ions  $Z_1$  and  $Z_2$ . In this case eqn. (44) becomes

$$- \frac{Z_1 Z_2}{(R_0 - x)^2} + \frac{Z_1^2}{(R_0 + x)^2} + \frac{1}{2} \frac{(Z_1 - Z_2) Z_1 x}{R_0^3} + \frac{1}{2} \frac{(Z_1 - Z_2) Z_1 (R_0 - x)}{R_0^3} = 0 \quad (47)$$

Performing easy algebraic manipulations we obtain the fifth degree equation

$$- 2x^5 + R_0 x^4 + 4R_0^2 x^3 - \frac{38}{5} R_0^4 x + 3R_0^5 = 0 \quad (48)$$

to be solved numerically. The solution has four complex roots and only one real with physical meaning, i.e.  $x = 0.4402 R_0$ . Therefore, in the case of carbon and hydrogen the new distance between two neighbouring ions is  $R'_0 = 0.56 R_0$ .

**(3) MCPs with electrons in the electrostatic force.** It is worth of interest to consider the case of MCPs, limited however to a mixture of C + O (the BCC configuration, Ichimaru 1982) and including the effects of electrons in the force balance. We consider an array of ions in the sequence O ( $Z_3$ ) - C ( $Z_1$ ) - H ( $Z_2$ ) - C ( $Z_1$ ) - O ( $Z_2$ ) as shown in the bottom panel of Fig. 5, and evaluate the displacement of the C nuclei bracketing the hydrogen nucleus by imposing the balance of electrostatic forces. In this case eqn. (4.2) becomes

$$- \frac{Z_1 Z_2}{(R_0 - x)^2} + \frac{Z_1 Z_3}{(R_0 + x)^2} + \frac{1}{2} \frac{(Z_1 - Z_2) Z_1 x}{R_0^3} + \frac{1}{2} \frac{(Z_1 - Z_2) Z_1 (R_0 - x)}{R_0^3} = 0 \quad (49)$$

the associated fifth degree equation is

$$- 10x^5 + 5R_0 x^4 + 20R_0^2 x^3 + 4R_0^3 x^2 - 46R_0^4 x + 19R_0^5 = 0 \quad (50)$$

where  $R_0$  is the distance between the C and O ions in the BCC lattice. Also in this case there is only one real solution,  $x = 0.4822 R_0$ . The distance between the C and H ions is therefore  $R'_0 = 0.5178 R_0$ .

**Implementing the correction into the reaction rates.** The effect of this correction on the interionic distance in the pycno-nuclear rates depends on the physical model for the rates. If we insert the new value of  $R_0$  into eqns. (40) and (41), the pycno-nuclear reaction of Salpeter & van Horn (1969) are enhanced by a large factor.

Using the Gasques et al. (2005), and Yakovlev et al. (2006) rates, in which the pycno-nuclear term is separate

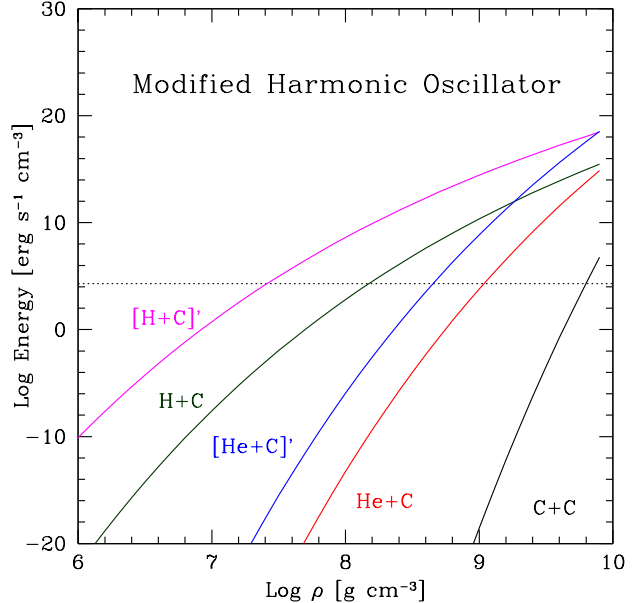


**Figure 3.** The energy generated by the reactions  $^{12}\text{C} + ^{12}\text{C}$  (blue line labelled C+C),  $^1\text{H} + ^{12}\text{C}$  (green line labelled H+C), and  $^4\text{He} + ^{12}\text{C}$  (red line labelled He+C) according to the MHO rates. The abundances by mass of C, H and He are  $\simeq 1$ ,  $10^{-21}$ , and  $3 \times 10^{-7}$ , respectively. This corresponds to an ideal WD made of sole carbon with traces of hydrogen or helium. The rates for the reactions  $^1\text{H} + ^{12}\text{C}$  (magenta line labelled [H+C]) and  $^4\text{He} + ^{12}\text{C}$  (cyan line labelled [He+C]) have been recalculated including also the effect on the local density caused by the presence of impurities as discussed in Section 4.2. Finally, the dotted black line represents the mean luminosity expressed in  $\text{erg s}^{-1} \text{cm}^{-3}$  of a typical WD. First all the rates intersect the mean luminosity which is the signature of a potential nuclear runaway, second the intersection occurs at higher and higher densities with increasing atomic number. Third, the effect of impurities is conspicuous (e.g. compare the green and magenta lines for hydrogen impurities or the red and cyan lines for He impurities).

from the thermal one, the functions  $a_{ij}$  must be redefined. Finally, the reaction rate Kitamura (2000) is more complicated to treat, because the temperature dependence is intrinsic in the formulation and cannot be singled out easily.

(i) *Gasques and Yakovlev rates.* There are two approximations depending on the composition of the plasma. If the plasma is made of pure  $^{12}\text{C}$  with  $^1\text{H}$  impurities, the new  $a_{ij}$  are

$$a_{ij} = \lambda \left[ \frac{3}{4\pi n} \right]^{1/3} \quad (51)$$

where  $\lambda = 0.56$  for the reaction  $^1\text{H} + ^{12}\text{C}$ , and  $\lambda = 0.73$  for the reaction  $^4\text{He} + ^{12}\text{C}$ . Other combinations of reactants (such as  $^1\text{H} + ^{16}\text{O}$ ) can be easily obtained from the general formalism above, and the effect of impurities is expected to be smaller. While using the rate by Salpeter & van Horn (1969), the correction is directly applied to  $R_0$ , using the Gasques et al. (2005) and Yakovlev et al. (2006) rates, the old  $a_{ij}$  coefficients of eqn. (11) are replaced by eqn. (51).

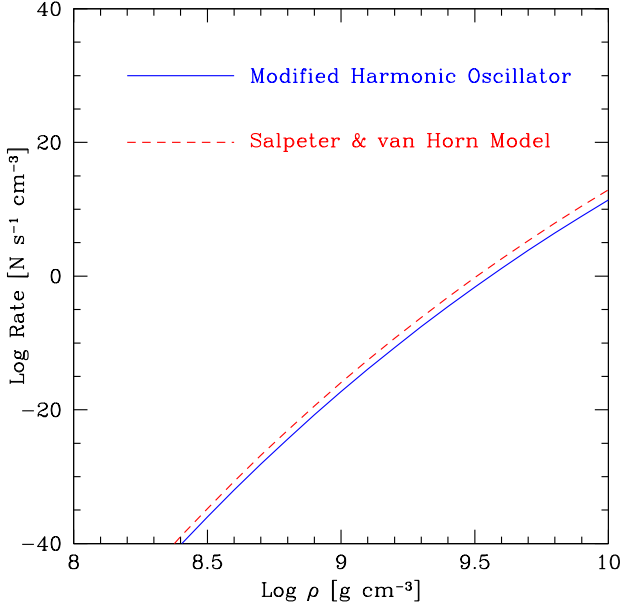


**Figure 4.**  $^{12}\text{C} + ^{12}\text{C}$  pycno-nuclear reaction rates for the simple MHO model (blue continuous line) compared with the Salpeter & van Horn (1969) model (red dashed line). They are roughly similar.

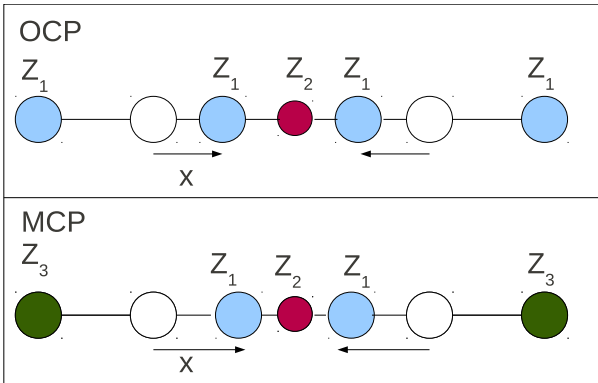


**Figure 5. Top Panel:** OCP made of carbon in which a nucleus of carbon ( $Z_1$ ) is replaced by a nucleus of hydrogen ( $Z_2$ ). We evaluate the forces acting on the nuclei  $Z_1$  adjacent to the impurity (charge  $Z_2$ ) and the corresponding displacement  $x$  of  $Z_1$  given by the new condition of force equilibrium. **Bottom Panel:** the same but for a MCP made of carbon and oxygen nuclei in BCC configuration in which a nucleus of oxygen is replaced by a nucleus of hydrogen.

$$a_{ij} = \frac{1}{2} \left[ \left( \frac{3Z_i}{4\pi n_e} \right)^{1/3} + \left( \frac{3Z_j}{4\pi n_e} \right)^{1/3} \right]. \quad (52)$$

In such a case the effect is less evident and smaller than before.

In the case of a MCP (for instance  $^{12}\text{C} + ^{16}\text{O}$ ), the new  $a_{ij}$  coefficients are

$$a_{ij} = 0.5178 a_{CO} = 0.5178 \frac{(6^{1/3} + 8^{1/3})}{2} \left[ \frac{3m_u}{4\pi 0.5\rho} \right]^{1/3} \quad (53)$$

where  $a_{CO}$  is derived from eqn. (52) above.

(ii) *Kitamura Rate.* In this case, at low densities the  $a_{ij}$  are those of the classical formulation given by eqn. (52), whereas at high density they must coincide with those of eqn. (4.2). In order to transit smoothly from the thermal to the pycno-nuclear regime and to take the correction of local densities due to impurities into account, we assume that the  $a_{ij}$  coefficients can be linearly interpolated in  $\log \rho$  according to

$$a'_{ij} = a_{ij}^{pyc} + (a_{ij}^{th} - a_{ij}^{pyc}) \frac{10 - \log \rho}{10 - 6} \quad (54)$$

where  $a_{ij}^{pyc}$  is defined according to eqn. (4.2) at  $\log \rho = 10$ , and  $a_{ij}^{th}$  is defined according to eqn. (52) at  $\log \rho = 6$ .

### 4.3 Results from the Modified Harmonic Oscillator

In the MHO formalism derived above, the total number of reactions per second per  $\text{cm}^3$  is given by

$$P_0 = n_{el} W \quad (55)$$

where  $n_{el}$  is the number density of the reacting elements. This is related to the abundance by number  $f_{el}$  by  $n_{el} = f_{el} N/V$  where  $N$  is the total number of ions in the star and  $V$  is the volume. In the simple case of reactions among identical ions, converting number densities to mass densities, mass abundances, and number abundances is straightforward, whereas in the case of reactions among different elements the procedure is more complicated. If  $N_j$ ,  $X_j$  and  $A_j$  are the number of ions of species  $j$  with mass abundance  $X_j$  and mass number  $A_j$ ,

$$X_j = \frac{N_j A_j m_u}{\sum N_i A_i m_u} \quad (56)$$

where  $m_u$  is the mass unit. If a WD, made of pure carbon, is polluted by traces of hydrogen and helium ( $N_H \ll N$  and  $N_{He} \ll N$ ) we obtain

$$X_H = \frac{f_H}{12} \quad \text{and} \quad X_{He} = f_{He} \frac{4}{12} = \frac{f_{He}}{3}. \quad (57)$$

For a WD of carbon and oxygen, whose mass abundances are related as  $X_C/X_O = \alpha$ , we derive

$$X_H = \frac{f_H}{12} \frac{[\alpha + (3/4)]}{(\alpha + 1)} \quad X_{He} = f_{He} \frac{4}{12} \frac{[\alpha + (3/4)]}{(\alpha + 1)} \quad (58)$$

for typical values of  $\alpha$ ,  $X_H$  is about a factor of 10 lower than  $f_H$ , and  $X_{He}$  is a factor of 3 lower than  $f_{He}$ .

Since the mass and structure of a WD depend on its central density, it is useful to express the reaction rates as a function of this parameter. In Fig. 3 we show the energy generation rates for the  $^1\text{H} + ^{12}\text{C}$ ,  $^4\text{He} + ^{12}\text{C}$  and  $^{12}\text{C} + ^{12}\text{C}$  reactions. These are calculated with the MHO rates with and without the impurities and associated density enhancement. We also show the case of the  $^{12}\text{C} + ^{12}\text{C}$  reaction calculated with the MHO. The astrophysical factors  $S(0)$  and  $Q$ -values of the

**Table 5.** Parameters for the nuclear reactions of hydrogen and helium with carbon.

	S(0) MeV barn	Q MeV
${}^1\text{H} + {}^{12}\text{C}$	$1.34 \times 10^{-3}$	1.94
${}^4\text{He} + {}^{12}\text{C}$	$1.00 \times 10^{-3}$	7.16

reactions  ${}^1\text{H} + {}^{12}\text{C}$ ,  ${}^4\text{He} + {}^{12}\text{C}$  are given in Table 5, those for the  ${}^{12}\text{C} + {}^{12}\text{C}$  are in Table 4. The abundances by number and by mass of the elements are  $f_{\text{H}} = 10^{-20}$ ,  $f_{\text{He}} = 10^{-6}$  and  $f_{\text{C}} = 1$  (or equivalently  $X_{\text{H}} = 10^{-21}$ ,  $X_{\text{He}} = 3 \times 10^{-7}$ , and  $X_{\text{C}} = 1$ ). For the sake of comparison we show also the mean luminosity of a typical CO-WD,  $10^{31} \text{ erg s}^{-1}$ . In order to express the energy generation rates and WD luminosity in units of  $\text{erg s}^{-1} \text{ cm}^{-3}$ , the WD luminosity is divided by the WD volume estimated assuming a mean radius of 5000 km.

The results of Fig 3 are of paramount importance: they clearly show that in the case of hydrogen impurities (with  $f_{\text{H}} = 10^{-20}$ ) the energy produced by the pycno-nuclear reactions at zero temperature may exceed the typical luminosity of a WD at a density  $\rho \simeq 3 \times 10^7 \text{ g/cm}^3$ , corresponding to a mass of about  $1.05 M_{\odot}$ , significantly smaller than the Chandrasekhar mass, see Table 1. This is a potentially explosive situation. In the case of helium, the intersection density and corresponding WD mass are higher but still of interest ( $\rho \simeq 4 \times 10^8 \text{ g cm}^{-3}$  and about  $1.3 M_{\odot}$ , respectively). Finally, the intersection with the  ${}^{12}\text{C} + {}^{12}\text{C}$  line is at about  $9.8 \text{ g cm}^{-3}$  and the corresponding WD mass is nearly equal to the Chandrasekhar limit.

As already discussed in Shapiro & Teukolsky (1983), the MHO expression for the reaction rate is not very different from the original one obtained by Salpeter & van Horn (1969) taking into account other effects, like electron screening and anisotropy. As a test, we compare the rates for the  ${}^{12}\text{C} + {}^{12}\text{C}$  reaction derived from the MHO above and Salpeter & van Horn (1969). The results are shown in Fig.4. The agreement is remarkable. Furthermore, these rates are also in good agreement with those by Gasques et al. (2005) for the same reaction.

## 5 CAN TRACES OF H AND HE BE PRESENT IN THE INTERIOR OF A WD?

The existence of traces of light elements in the core of CO-WDs is at the basis of our investigation. Light elements are the best candidates to consider, because the very high coulombian barriers of high  $Z$  elements would quench the penetration probabilities to zero.

Undoubtedly, hydrogen and helium on the WD surfaces in small but significant abundances are predicted theoretically ( $10^{-9} \leq X_{\text{H}} \leq 10^{-5}$  according to Miller Bertolami et al. 2013; Renedo et al. 2010) and are observed (Bergeron et al. 1990). How much hydrogen or helium can be present in the interior?

Following Kippenhahn & Weigert (1990), the rather high internal temperatures (from  $10^8$  to  $10^6$  K) of an aging WD set a limit to the possible hydrogen content in the interior. If hydrogen were present with a mass concentra-

tion  $X_{\text{H}}$ , we would expect H-burning via the pp-chain. For average values  $T = 5 \times 10^6$  K,  $\rho = 10^6 \text{ g cm}^{-3}$ , the energy released by the pp-chain  $\epsilon_{pp} \simeq 5 \times 10^4 X_{\text{H}}^2 \text{ erg g}^{-1} \text{ s}^{-1}$  to which for a  $M = 1 M_{\odot}$  the luminosity would be  $L/L_{\odot} \simeq M/M_{\odot} \times \epsilon_{pp} \simeq 2.5 \times 10^4 X_{\text{H}}^2$ . The mean observed luminosity of WD  $L/L_{\odot} \simeq 10^{-3}$  allows  $X_{\text{H}} \leq 2 \times 10^{-4}$ , the upper limit for  $X_{\text{H}}$  in WD interiors. Stability considerations indeed rule out that the luminosity of normal WD is generated by thermonuclear reactions, which was first pointed out by Mestel (1952b,a). Nuclear burning could only be expected in nearly cold configurations near  $T = 0$  by pycno-nuclear reactions.

According to Kawaler (1988) sedimentation and diffusion of elements will bring hydrogen and helium from the interior to surface and viceversa. Although this is a slow process, the initial content of hydrogen can be as high as  $10^{-6} M_{\odot}$ . It is worth noting that diffusion of hydrogen inwards is inhibited by the electron degeneracy (see for instance Iben & MacDonald 1985). In brief, while the tail of the hydrogen distribution chemically diffuses inward as the WD cools down, actually it may reach a maximum depth, and with further cooling, begins to retreat outwards. This is because the increasing electron degeneracy halts the inward diffusion of hydrogen. Hence, surface hydrogen never reaches very deep layers.

We argue and try to demonstrate here that traces of light elements (below the upper limits given above) left over by core nuclear burnings during the previous phases can still be present when the WD is cooling. This would be the analog of the situation in neutron stars, where traces of electrons, protons and even heavy nuclei are expected to exist in the medium of free neutrons (Shapiro & Teukolsky 1983). We show that hydrogen abundances in the range  $10^{-22} \leq X_{\text{H}} \leq 10^{-14}$  may be present and cause ignition of pycno-nuclear reactions. Analogous considerations can be made for helium.

### 5.1 Hydrogen and helium contents expected in stellar interiors at the end of the AGB phase

The correct answer to the above question would be detailed numerical models of stellar interiors in which the abundances of all elements undergoing nuclear processing, convective mixing, diffusion and sedimentation (whenever appropriate) are followed in a great detail to even very low values. In current stellar models, the abundances of the chemical elements are calculated by solving complicated networks of differential equations governing the local creation / destruction of the elemental abundances according to the rates of the nuclear reactions that are involved, and the efficiency of the diffusive/convective mixing.

A widely adopted short-cut to the above complex integration technique and quite heavy computational burden is to set equal to zero the abundances of elements when they fall below some reasonably small values, unless otherwise required. This is particularly true for those elements that initially are very abundant, such as hydrogen and helium. They indeed are customarily set to zero when  $X_{\text{H}} \simeq 10^{-8}$  and  $X_{\text{He}} \simeq 10^{-8}$ . In the case of the central H- and He-burnings this is also taken to mark the end of the evolutionary phase (see for instance Bertelli et al. 1994; Bressan et al. 2012, and references therein) when describing the physical ingredients and technical details of the Padova stellar evolutionary code. Furthermore, requesting that all elements that are

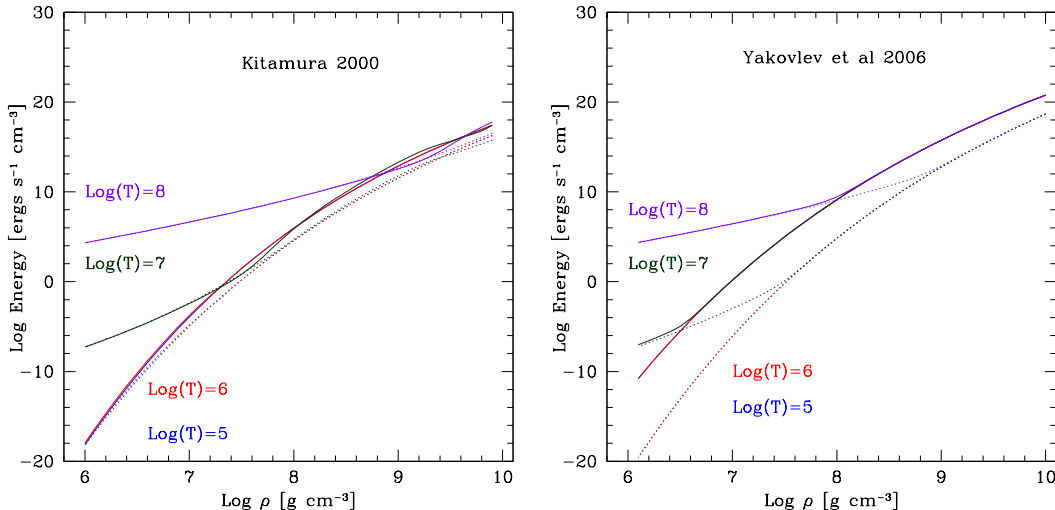


**Figure 6.** **Left Panel:** energy rates per unit volume produced by the reaction  $^{12}\text{C}(^1\text{H}, \gamma)^{13}\text{N}$  with hydrogen abundance  $X_{\text{H}} = 10^{-20}$  as a function of density and four different temperatures of the thermal branch. The nuclear rates are from Kitamura (2000). The dotted lines represent the energy without local density correction while the continuous lines represent the model that considers local density correction. **Right panel:** the same as in the left panel but for reaction rates according to Yakovlev et al. (2006). The dotted lines represent the energy without local density correction while the continuous lines represent the model that considers local density correction.

gradually transformed into heavier species (and therefore decrease their abundance) are followed to extremely low values is hardly viable and time consuming when extended grids of stellar models are considered. Therefore, proving or disproving that traces of hydrogen and helium (at the abundances that will be used in the present study) can survive previous burnings and be present in WDs cannot be easily assessed with current evolutionary codes to disposal.

However, the elementary theory of thermo-nuclear reactions suggests that elements at very low abundances can survive even the nuclear phase in which they are burned into heavier species. In brief, looking at the case of hydrogen, the typical lifetime of a proton against a proton in the pp-chain or against CNO nuclei in the CNO-cycle is expected to decrease with increasing the temperature and to increase with decreasing  $X_{\text{H}}$  (see Iben 2013a,b). In other words, as the abundance of hydrogen decreases, it is more and more difficult to destroy it further, i.e. the abundance of hydrogen never becomes zero. Similar considerations can be made for helium (and any other element in general).

We try here two simple experiments designed to estimate the abundances  $X_{\text{H}}$  and  $X_{\text{He}}$  left from the nuclear burnings along the whole evolutionary history from the zero age main sequence to the beginning of the TP-AGB phase that terminates with generation of CO WD (the TP-AGB phase can be neglected because of its short lifetime compared to that of previous phases). Hydrogen and helium expected in WDs have survived all previous nuclear burnings.

To this aim we consider the evolutionary sequences of the 3, 5 and 6  $M_{\odot}$  stars with solar-like composition [ $X=0.723$ ,  $Y=0.260$ ,  $Z=0.017$ ] that are the progenitors of massive CO WDs e.g. the entries of Table 2. The sequences are taken from the Padova library of stellar models by Bertelli et al. (2009). For each star we know all relevant physical quantities as a function of time both in the centre (temperature, density, abundances of elements, size of

the convective and H-exhausted core, etc.) and at the surface (total and partial luminosities, effective temperature, etc.).

Since the central H- and He-burning (CNO and  $3\alpha$ , respectively) in these stars are point-like sources at the centre, we may use simple energy conservation arguments and write

$$\epsilon_i(X_i, T, \rho) = \frac{L_i}{M} \quad (59)$$

where the index  $i$  stands for H- or He-burning, and  $L_i$  are the partial luminosities (the total luminosity is  $L = L_{\text{H}} + L_{\text{He}} + L_{\text{G}}$ , where  $L_{\text{G}}$  is the contribution from gravitational contraction, usually negligible). This equation simplifies the complexity of energy production (nuclear burning and gravitational release in convective/radiative conditions, the latter depending on the stellar mass) to an ideal situation in which a gram of matter produces the amount of energy radiated by the surface per unit mass and unit time. Using the above equation we implicitly neglect the contribution of the gravitational contraction/expansion to the luminosity (a reasonable approximation for most of the stellar lifetime). Furthermore, for the sake of simplicity, we consider only the nuclear burning occurring in the core and ignore the nuclear burning in the shell. In the 3, 5, 6  $M_{\odot}$  stars, hydrogen burns via the CNO-cycle with a small contribution from the pp-chain, and helium burns via the  $3\alpha$  process. Finally, in first approximation we consider nuclear burning only in radiative conditions, neglecting continuous refueling by convection which may occur in stars of 3, 5 and 6  $M_{\odot}$ .

For the energy release by H- and He-burning we adopt analytical expressions from classical textbooks (Kippenhahn & Weigert 1990; Weiss et al. 2004):

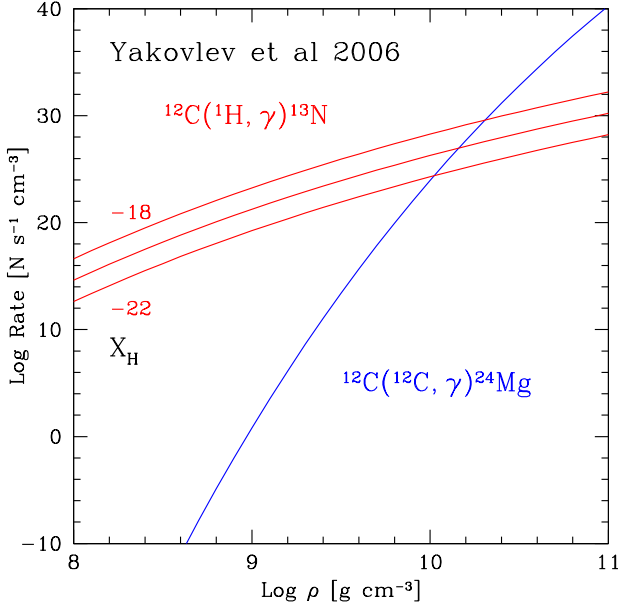


**Figure 7.** We compare the rates of the pycno-nuclear reactions  $^{12}\text{C}(^1\text{H}, \gamma)^{13}\text{N}$  (dashed red lines) and  $^{12}\text{C}(^{12}\text{C}, \gamma)^{24}\text{Mg}$  (solid blue line) according to the rates by Yakovlev et al. (2006) and different values of  $X_{\text{H}}$  as indicated. From top to bottom  $\log X_{\text{H}} = -18, -20$  and  $-22$ .

(i) pp-chain,

$$\begin{aligned} \epsilon_{pp} &= 2.06 \times 10^6 f_{pp} g_{pp} \rho X_{\text{H}}^2 T_6^{-0.66} e^{(-33.81 T_6^{-0.33})} \\ g_{pp} &= 1 + 0.0012 T_6^{0.33} + 0.0078 T_6^{0.66} + 0.0006 T_6 \\ f_{pp} &= 1 + 0.25 \rho^{0.5} T_6^{-1.5} \end{aligned} \quad (60)$$

(ii) CNO-cycle

$$\begin{aligned} \epsilon_{\text{CNO}} &= 8.7 \times 10^{27} g_{14,1} X_{\text{CNO}} X_{\text{H}} \rho T_6^{-2/3} e^{-152.28/T_6^{1/3}} \\ g_{14,1} &= 1 + 0.003 T_6^{1/3} - 0.0078 T_6^{2/3} - 0.00015 T_6 \end{aligned} \quad (61)$$

(iii) and  $3\alpha$

$$\begin{aligned} \epsilon_{3\alpha} &= 5.09 \times 10^{11} f_{3\alpha} X_{\text{He}}^3 \rho^2 T_8^{-3} e^{(-44.027/T_8)} \\ f_{3\alpha} &= \exp(2.4 \times 10^{-3} \rho^{1/2} / T_8^{3/2}) \end{aligned} \quad (62)$$

where  $T_6$  and  $T_8$  are the temperatures in units of  $10^6$  and  $10^8$  K, respectively, the functions  $g_{14,1}$  and  $g_{3\alpha}$  are the screening factors,  $X_{\text{H}}$ ,  $X_{\text{He}}$ ,  $X_{\text{CNO}}$  are the abundances by mass of hydrogen, helium and CNO group, respectively;  $\epsilon$ , and  $\rho$  are in cgs units,  $\text{erg g}^{-1} \text{s}^{-1}$  and  $\text{g cm}^{-3}$ , respectively; finally, the above expressions refer to situations in which all intermediate steps are at equilibrium.

(i) **Analytical.** An estimate of the hydrogen abundance left from the nuclear burning after the main sequence and the helium burning phase can be given analytically in the following way considering the relative weigh of pp-chain and CNO-cycle in the H-burning process. Let  $X_{\text{H},r}$  be the hydrogen abundance at a certain time  $t$ . At proceeding nuclear burning over a time interval  $\Delta t$ , the fraction of consumed hydrogen is  $X_{\text{H},c} = X_{\text{H},i} - X_{\text{H},r}$ , where  $X_{\text{H},i}$  is the initial abundance of hydrogen. Therefore  $\Delta X_{\text{H},c} = -\Delta X_{\text{H},r}$ . The

**Table 6.** Hydrogen abundances in the innermost regions at the end of the Main Sequence and core He-burning, and beginning of the TP-AGB phases according to two simple models.

Mass	Phase	$X_{\text{H}}$	$X_{\text{H}}$
		Analytical	Numerical
$3 M_{\odot}$	Hb	$2.9 \times 10^{-4}$	$1.7 \times 10^{-7}$
	Heb	$3.6 \times 10^{-9}$	$1.3 \times 10^{-14}$
	AGB	$2.4 \times 10^{-13}$	$3.3 \times 10^{-18}$
$5 M_{\odot}$	Hb	$8.8 \times 10^{-5}$	$2.4 \times 10^{-7}$
	Heb	$2.7 \times 10^{-9}$	$4.2 \times 10^{-14}$
	AGB	$1.2 \times 10^{-12}$	$7.8 \times 10^{-18}$
$6 M_{\odot}$	Hb	$3.7 \times 10^{-5}$	$2.8 \times 10^{-7}$
	Heb	$2.2 \times 10^{-9}$	$7.3 \times 10^{-14}$
	AGB	$1.9 \times 10^{-12}$	$1.2 \times 10^{-17}$

fraction  $X_{\text{H},c}$  is in turn governed by the equation

$$\frac{\Delta X_{\text{H},c} \rho}{m_p} = \frac{\epsilon \rho \Delta t}{Q} \quad (63)$$

where  $\epsilon$  is a function of  $X_{\text{H},r}$ . In particular for the case of the pp-chain,  $\epsilon$  it is proportional to  $X_{\text{H},r}^2$ . Therefore we can write in differential form

$$-\frac{dx}{x^2} = A_{pp} dt \quad (64)$$

where  $x$  stands for the current value of  $X_{\text{H},r}$ . Upon integration we obtain

$$x_f = \frac{1}{\frac{1}{x_i} + A_{pp} \Delta t} \quad (65)$$

where  $x_i$  and  $x_f$  are the values of  $X_{\text{H},r}$  at the beginning and at the end of the generic time step.

In the case of the CNO-cycle  $\epsilon$  is a linear function in  $X_{\text{H},r}$ . Therefore we have

$$-\frac{dx}{x} = A_{cno} dt \quad (66)$$

that gives

$$x_f = x_i e^{-A_{cno} \Delta t} \quad (67)$$

Taking the weighted mean value of the two channels and extending the integration over the whole time interval from the zero age main sequence to the end of he-burning, we obtain

$$\langle X \rangle = \frac{A_{pp} X_{\text{H}}^{pp} + A_{cno} X_{\text{H}}^{cno}}{A_{pp} + A_{cno}} \simeq 10^{-12} - 10^{-13} \quad (68)$$

for a progenitor from 3 to  $6 M_{\odot}$ . The evolutionary history of the stars comes in via the central temperature and density as functions of the time. The results for the central hydrogen content along the evolutionary sequences are shown in Table 6.

(ii) **Numerical.** The above result can be refined making use of eqn. (59), considering that in principle the pp-chain and CNO-cycle can occur simultaneously, however with significantly different efficiency, and taking into consideration the structure of the stars during their evolutionary history. In principle if one or more nuclear burning regions are present in a star, eqn. (59) implies

$$\sum_i \int_0^M \sum_j \epsilon_{i,j} dm = \sum_i L_i \quad (69)$$

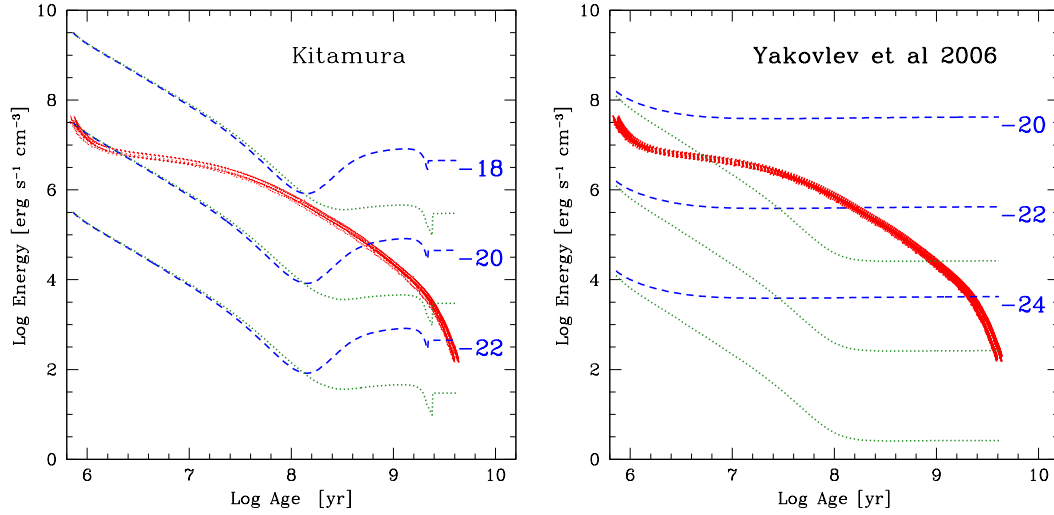


**Figure 8. Left Panel:** We plot the pycno-nuclear energy generation rates based on the Kitamura (2000) model for the reaction  $^{12}\text{C}(^1\text{H}, \gamma)^{13}\text{N}$  and three different values of hydrogen (from  $X_{\text{H}} = 10^{-18}$  to  $X_{\text{H}} = 10^{-22}$ ) as shown by the blue continuous lines and compare these with the luminosity of the WD (red dotted line) according to the models of Althaus & Benvenuto (1997, 1998) for a  $1.2 M_{\odot}$  WD. The released nuclear energy and WD luminosity are per unit volume in units of  $\text{erg s}^{-1} \text{cm}^{-3}$ . To do so, the luminosity of the WD is divided by the WD volume using the data provided by Althaus & Benvenuto (1997, 1998). The nuclear rates are calculated using the central values of temperature and luminosity of the WD model we have adopted. The green lines represent the energy without local density correction while the blue lines represent the model that considers local density correction. **Right Panel:** the same as in the left panel but for the nuclear energy rates based on the Yakovlev et al. (2006) and different values of  $X_{\text{H}}$  from  $X_{\text{H}} = 10^{-20}$  to  $X_{\text{H}} = 10^{-24}$ .

where  $i$  indicates the phase, and  $j$  the type of burning (pp, CNO, and  $3\alpha$  as appropriate). If only central H-burning is present (main sequence), eqn. (69) reduces to  $\epsilon_{\text{H}} \times M = L_{\text{H}}$ ; when central and shell H-burnings are present it becomes  $\epsilon_{\text{H},\text{core}} \times M_{\text{core}} + \epsilon_{\text{H},\text{shell}} \times M_{\text{shell}} = L_{\text{H},\text{core}} + L_{\text{H},\text{shell}} = L_{\text{H}}$ ; with more complicated nuclear stratifications and phases the generalization of eqn. (69) is obvious. The first case is simple to treat and  $L_{\text{H}}$  is the true luminosity generated by core H-burning. The second case is more complicated and cannot be solved analytically for obvious reasons. Fortunately, some approximation are possible: first compared to the main sequence lifetime it is short lived and can be neglected. To this aim we have remove the contribution to the nuclear energy generation by the the shell and suitably rescaled the luminosity  $L_{\text{H}}$  (this is possible because all details of the stellar models are to our disposal).

In the case of central core H-burning, isolating the dependence on  $X_{\text{H}}$  in eqns. (61) and (62), we can write

$$\epsilon_{\text{pp}} + \epsilon_{\text{cno}} \simeq \epsilon_{\text{pp}}^o X_{\text{H}}^2 + \epsilon_{\text{cno}}^o X_{\text{H}} = L_{\text{H},\text{core}}/M \quad (70)$$

where the quantities with superscript  $o$  are of obvious definition and are immediately known from eqns. (61) and (62), and  $L_{\text{H},\text{core}}$  is the contribution to the total luminosity by the sole core H-burning. This quantity is known from the stellar models we are using. Eqn. (70) is a second order algebraic equation to be solved for  $X_{\text{H}}$  as a function of the temperature and density of the mass element (typically a small volume at the center) along the evolutionary sequence of a star. The results at the end of the core H-burning, core He-burning, and beginning of the TP-AGB phase are listed in Table 6.

Similar reasoning can be followed to derive the helium

abundance. We recast eqn. (70) as

$$\epsilon_{3\alpha} = \epsilon_{3\alpha}^o X_{\text{He}}^3 = L_{\text{He},\text{core}}/M \quad (71)$$

and solve it for  $X_{\text{He}}$ . With this procedure we estimate that the abundance of helium in the core at the start of TP-AGB phase is about  $X_{\text{He}} = 10^{-6}$  in the three stellar models.

No estimate is made of the amounts of central hydrogen and helium consumed during the TP-AGB phase because of the complexity of the stellar evolution during this phase. However, this is less of a problem because the TP-AGB is short-lived compared to the previous evolutionary history so that it can be neglected.

## 5.2 Decrease of $X_{\text{H}}$ and $X_{\text{He}}$ during the WD cooling sequence

At the beginning of the WD cooling sequence the luminosity is sustained by CNO burning on the surface. We want to assess whether part of the luminosity may still be due to minor nuclear burning in the interior (if it can occur at all), thus possibly further lowering the inner content of hydrogen. In order to follow the hydrogen and helium consumption by nuclear burnings during the early stages of WD cooling, we used the WD evolutionary sequences of Renedo et al. (2010) in which the surface burnings (in the H and He-shells) are followed in great detail so that they can be taken as a reference models. Using the same procedure described above, we estimate that the central hydrogen and helium abundances in our test models of 3, 5 and  $6 M_{\odot}$  during the time interval in which the surface shells are active, approximately  $\sim 4 \times 10^6$  yr, decrease only by a modest amount (roughly less than a factor of 10), i.e. the new abundances are  $X_{\text{H}} = 10^{-19} - 10^{-18}$  and  $X_{\text{He}} = 10^{-7}$ .



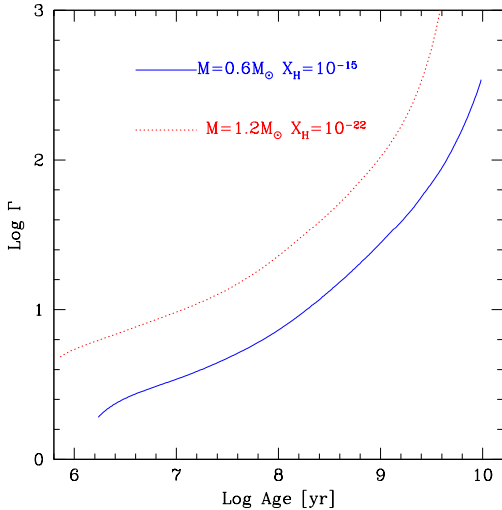


**Figure 9.** The Coulomb coupling parameter  $\Gamma_{ij} = \frac{Z_1 Z_2 e^2}{a_{ij} k_B T}$  as function of age for the two extreme values of the WD masses under consideration. The underlying nuclear reaction is  ${}^1\text{H} + {}^{12}\text{C}$ . The enhancement in the local density induced by the contaminant hydrogen is included (see eqn. 48 and the solution  $R'_0 = 0.5178 R_0$ ). The blue lines show the  $0.6M_\odot$  WD with  $X_{\text{H}} = 10^{-15}$ , whereas the red lines are the same but for the  $1.2M_\odot$  WD with  $X_{\text{H}} = 10^{-22}$ . All other combinations of mass and  $X_{\text{H}}$  abundances fall in between. The corresponding Coulomb coupling parameter with no enhancement in the local density are obtained by scaling the values on display by the factor  $1/0.5178$ .

### 5.3 General Remarks

To conclude, the experiment and arguments presented above suggest that traces of hydrogen and helium can be left over in the interiors of a WD at the end of the whole nuclear history via the thermal channels of nuclear reactions. However it is worth emphasizing that major drawbacks and uncertainties are present. In brief

(i) There is a large difference between the results obtained with the two methods. We prefer to consider those from the numerical approach to be more realistic because they are tightly related to detailed stellar models (temperatures, densities and luminosities).

(ii) We have used the classical reactions rates for the pp-chain, CNO-cycle and  $3\alpha$  group at the equilibrium. This prevents us from following the temporal history of the abundances of the intermediate elements and reactions. To highlight the issue, if some hydrogen survives the stage of core H-burning, we would expect that any trace of hydrogen should be completely burnt during the helium core burning, as a result of the reactions  ${}^{12}\text{C} + \text{H} \rightarrow {}^{13}\text{C}$  and  ${}^{13}\text{C} + \text{H} \rightarrow {}^{14}\text{N}$ . Eventually, all  ${}^{14}\text{N}$  should be converted into  ${}^{22}\text{Ne}$  via  $\alpha$ -captures. This sequence of events cannot be described correctly by our CNO-cycle equilibrium rates. This is perhaps the point of major uncertainty.

(iii) Detailed evolutionary models would be the right way of assessing whether traces of light elements could be present in the interiors of WDs at the beginning of their cooling sequence and, if so, whether there exists any trend and/or lower limit at varying the initial mass of the progenitor star.

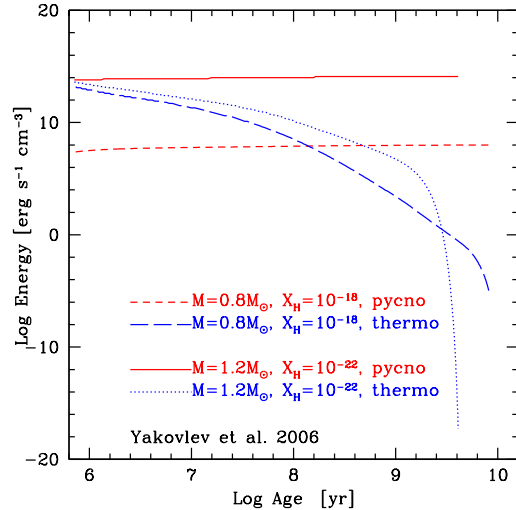


**Figure 10.** The nuclear energy rates  $R_{ij}(\rho, T) = R_{ij}^{pyc}(\rho) + \Delta R_{ij}(\rho, T)$  of Yakovlev et al. (2006). The first term is the pycno contribution (short dashed and solid red lines) and the second one the thermal component (long dashed and dotted blue lines). Two values of the WD mass and two values of  $X_{\text{H}}$  are displayed, i.e.  $0.8M_\odot$  with  $X_{\text{H}} = 10^{-18}$  and  $1.2M_\odot$  with  $X_{\text{H}} = 10^{-22}$ . The energy generation rates are in  $\text{erg cm}^{-3} \text{s}^{-1}$ .

(iv) An alternative to calculating complete stellar models could be the ideal case of an elementary cell of matter in which extended networks of nuclear reactions among a number of elementary species are let occur as a function of temperature, density and patten of initial chemical parameters. To simulate the centre of a real star, temperature and density as a function of time could be taken from detailed stellar models.

Work is in progress along the lines of items (iii) and (iv).

Despite the above limitations of the present approach and waiting for careful numerical investigations, we consider the above estimates of  $X_{\text{H}}$  and  $X_{\text{He}}$  as *free parameters* within the ranges we derived above, and proceed to investigate the effects they would induce on the evolution of WDs of different mass.

## 6 RESULTS FOR THE KITAMURA AND YAKOVLEV REACTION RATES

The Kitamura (2000), Gasques et al. (2005) and Yakovlev et al. (2006) formalisms (see also Beard 2010) were originally tailored for reactions like  ${}^{12}\text{C} + {}^{12}\text{C}$ ,  ${}^{12}\text{C} + {}^{16}\text{O}$ ,  ${}^{16}\text{O} + {}^{16}\text{O}$ . However, they can be extended to reactions involving impurities of light elements, and to incorporate the enhancement in the local density. We have used the reaction rates of Kitamura (2000) to study the reactions  ${}^1\text{H} + {}^{12}\text{C}$  and/or  ${}^4\text{He} + {}^{12}\text{C}$ . We will not examine here the similar reactions occurring with oxygen because of the higher atomic number  $Z$ . The relative  $S$  factors and  $Q$  values of the two reactions are listed in Table 5. The abundance of carbon in these test calculations is  $X_{\text{C}} \simeq 1$ . The results are more general than those of the Salpeter & van Horn (1969) rates because they take also into account the effects of the temperature, extending from the thermal to the

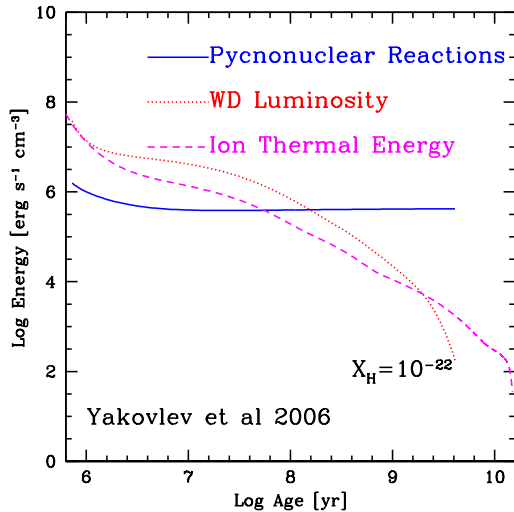


**Figure 11.** The pycno-nuclear energy rates based on the Yakovlev et al. (2006) model for an abundance concentration of hydrogen  $X_H = 10^{-22}$  (blue continuous line) compared to the luminosity of the WD (red dotted line) according to the models of Althaus & Benvenuto (1997, 1998) for a  $1.2 M_\odot$  WD. The dashed magenta line represents the energy of the ions. The luminosity is in the same units as the energy generation rates ( $\text{erg cm}^{-3} \text{s}^{-1}$ ).

pycno-nuclear regime. However, our results match those obtained with the Salpeter & van Horn (1969) rates in the low temperatures and high densities regime. Results for the  $^{12}\text{C}(^1\text{H}, \gamma)^{13}\text{N}$  reaction with  $X_H = 10^{-20}$  are presented in left panel of Fig. 6, in which the generated energy is plotted as a function of central density. The same procedure has been applied to the Yakovlev et al. (2006) formalism. The results for the same reaction and hydrogen abundance are shown in the right panel of Fig. 6. In both cases, four different temperatures have been considered.

In both panels the thermal branches are visible only for the  $10^7$  and  $10^8$  K temperatures. All curves merge together beyond a certain value of the density that depends on the temperature and source of the rates. The two groups of rates significantly differ both in the thermal and pycno-nuclear regime: the Kitamura (2000) rates are higher in the thermal and lower in the pycno-nuclear regime compared to those Yakovlev et al. (2006). The rates are enhanced by the increase in the local density. This dependence is shown by the results in Fig. 7 which displays the  $^1\text{H} + ^{12}\text{C}$  and  $^{12}\text{C} + ^{12}\text{C}$  reaction rates, limited to the case of Yakovlev et al. (2006), for three values of  $X_H$  as indicated. These results can be compared to those of Fig. 3, scaled to the same energy units and multiplied by the  $Q$ -value. The energy generation rate exceeds the mean luminosity of a WD at relatively low densities.

## 7 INCLUDING THE REAL EVOLUTION OF A WD

WDs of given masses follow cooling sequences along which the luminosity varies with time. Therefore we relax now the simplifying assumption of a constant mean luminosity by using the evolutionary sequences of WDs of different mass and

compare them with the energy released by nuclear burning. The cooling sequence in the luminosity vs effective temperature plane is determined by the central density and mean molecular weight of the electrons (i.e. the chemical composition of the WD). Therefore the really meaningful comparison is between the energy production of the WD governed by its temperature and density (the central values) and its current luminosity.

**Taking the WD structure into account.** In our analysis we need to compare the total luminosity with the total nuclear energy generation inside ( $L \equiv \int \epsilon dM$ ) along the cooling sequence. To this aim we need the internal structure of the WD. The cooling sequence provides the age from the beginning of the WD phase, the luminosity, effective temperature, and the central temperature and density. At each stage we integrate the structure equations of a WD of given mass, chemical composition, and central density in the so-called zero-temperature approximation. This provides the stratification of mass and density as functions of the radius. Owing to the high thermal conductivity of degenerate electrons (see below), the temperature tends to become more and more uniform from the center to the surface at increasing age of the WD (lowering of the mean temperature by cooling). In order to evaluate the reaction rate as a function of the position it is sufficient to assume that the temperature throughout the star is equal to its central value. This may not be correct toward the surface, but the reaction rates are nearly zero over there because of the low density (the nuclear energy production, if any takes place, is mostly limited to the central regions). Therefore we assume that the rate of energy production along the radial distance is  $\epsilon[T_c, \rho(r)]$ , and proceed to calculate the mean energy production per unit volume,  $\langle \epsilon \rangle$ , and unit mass,  $\langle \frac{\epsilon}{\rho} \rangle$ . The luminosity per unit volume of a WD is given by

$$\frac{L}{V} = \frac{4\pi R^2 \sigma T_{eff}^4}{V} \quad (72)$$

where  $V$  is the total volume of the WD. This luminosity must be compared with

$$\langle \epsilon \rangle = \frac{\int_0^R \epsilon[T_c, \rho(r)] \times 4\pi r^2 dr}{\int_0^R 4\pi r^2 dr} \quad (73)$$

in  $\text{erg cm}^{-3} \text{s}^{-1}$ .

In addition to this we will make use of the energy generated per unit mass and time given by

$$\langle \frac{\epsilon}{\rho} \rangle = \frac{\int_0^R \epsilon[T_c, \rho(r)] \rho^{-1} \times 4\pi r^2 dr}{\int_0^R 4\pi r^2 dr} \quad (74)$$

in  $\text{erg g}^{-1} \text{s}^{-1}$ .

These quantities can be expressed by those evaluated at the center  $[\epsilon]_c$  and  $[\frac{\epsilon}{\rho}]_c$  by means of the relations  $\langle \epsilon \rangle = [\epsilon]_c (V_c/V)$  and  $\langle \frac{\epsilon}{\rho} \rangle = [\frac{\epsilon}{\rho}]_c \times (V_c/V)$ , where  $V_c$  is the volume of a small sphere of radius  $R_c$  around the center. The radius  $R_c$  is found to range from  $6.5 \times 10^7$  to  $2.5 \times 10^7$  cm when the WD increases from  $0.6$  to  $1.2 M_\odot$  mass. This radius is about a factor  $1/20$  smaller than the real radius of WDs of the same mass. This means that the nuclear energy is mainly generated in a small sphere around the center, thus justifying the approximation  $\langle \epsilon \rangle \simeq \epsilon_c \times (V_c/V)$  and  $\langle \epsilon/\rho \rangle \simeq (\epsilon_c/\rho_c) \times (V_c/V)$ .

**Results.** For the sake of illustration, let us consider the evolutionary sequence of a CO-WD of  $1.2 M_{\odot}$  (the border value above which the mean density is high enough to enter the General Relativity domain) calculated by Althaus & Benvenuto (1997, 1998). All necessary information about central temperature, central density and luminosity, etc is available. The composition of the WD is  $X_C \simeq 0.5$  and  $X_O \simeq 0.5$ . We are particularly interested in determining when the energy rates given by Kitamura (2000) or by Yakovlev et al. (2006), modified for the effects of contaminants on the local densities, exceed the luminosity. Fig. 8 shows the variation of the WD luminosity (the red thick dotted curve) as a function of time and the energy generated by the reaction  $^{12}\text{C}(^1\text{H}, \gamma)^{13}\text{N}$  for different abundances  $X_H$  and keeping  $X_C$  constant (the thin dashed blue and the thin dotted green curves). The dotted green lines are for nuclear rates that neglect the local density enhancement caused by impurities, whereas the dashed blue lines are for nuclear rates that take this into account.

There are a number of important points to note:

(i) When the enhancement in local density is not considered, the nuclear rates show a similar trend, they initially decrease, but at given WD age they become flat (see the green curves in both panels of Fig. 8). The little kick in the Kitamura (2000) rates is a numerical artefact in his relations passing from fluid to solid state. The initial decrease of the nuclear rate is the signature of the thermal regime and that the main source of energy is the internal energy of the ions, whereas the levelling of the rate is when the pycno-nuclear regime takes over.

(ii) When the enhancement in local density is taken into account, this trend is only typical of the Kitamura (2000) rates. This is partially because we used a linear interpolation to calculate the interionic distance in transiting from the low-density, thermal regime to the high-density pycno-nuclear regime (see eqn. 4.2). The nuclear rates of Yakovlev et al. (2006) are nearly flat all over the age range. The pycno-nuclear regime dominates the rate from the very beginning. This is partially due to the mass we have chosen in which the density is very high ( $\rho_c \simeq 1.8 \times 10^8 \text{ g cm}^{-3}$  for the  $1.2 M_{\odot}$  WD). For lower masses the previous trend is recovered.

(iii) For the Kitamura (2000) model the pycno-nuclear energy exceeds the luminosity of the WD for  $X_H = 10^{-21}$  after 6 Gyr (see the left panel of Fig. 8). Assuming instead the Yakovlev et al. (2006) rates, we reach the critical situation for  $X_H = 10^{-22}$  even before 1 Gyr (see the right panel of Fig. 8).

To clarify the above issues first we examine the variation of the Coulomb coupling parameter  $\Gamma_{ij}$  along the cooling sequences of the WD models.  $\Gamma_{ij}$  for the  $^1\text{H} + ^{12}\text{C}$  reaction is shown in Fig.9. It is soon evident that the reaction occurs in the third and fourth regimes of the group of five that have been discussed in Section 3.3 as long as the age is younger than 1 Gyr for the  $1.2 M_{\odot}$  and 8 Gyr for the  $0.6 M_{\odot}$ , respectively. More precisely, initially the nuclei are bound to the lattice sites, so that the reaction occurs between highly thermally excited nuclei, which oscillate with frequencies higher than the plasma frequency and have energies greater than the zero point energy of the plasma; later they enter the so-called thermally enhanced pycno-nuclear regime but the

melting temperature is not reached yet. Only WDs older than the above limits enter the pure pycno-nuclear regime.

Second we look at the separate contributions to the total rate by the thermally enhanced and pure pycno-nuclear regimes according to the Yakovlev et al. (2006) formalism. In eqn. (26), the total rate is made by the sum of two terms  $R_{ij}(\rho, T) = R_{ij}^{pyc}(\rho) + \Delta R_{ij}(\rho, T)$ , where the first term is the pycno contribution and the second one the thermal component. The evaluation is made for two values of the WD mass and two values of  $X_H$ , i.e.  $0.8 M_{\odot}$  with  $X_H = 10^{18}$  and  $1.2 M_{\odot}$  with  $X_H = 10^{-26}$ . The results are shown in Fig. 10, where the blue long dashed and dotted curves are for the thermally enhanced component, and the red short dashed and solid curves are for the pure pycno component, respectively.

As already anticipated, the contribution from the thermally enhanced channel is significant for the  $0.8 M_{\odot}$  WD, it gradually decreases as the WD mass (density) increases, and is fully masked by the pycno-nuclear one for the  $1.2 M_{\odot}$  star and beyond.

## 7.1 Adding up all sources of energy: critical $X_H$ abundances and ages

We now include all energy sources, i.e. the generation by any of the five possible regimes for the pycno-nuclear reactions (including also the so-called thermally enhanced terms in the early stages of WD cooling sequences) and the thermal energy of the ions.

**The proto-type WD of  $1.2 M_{\odot}$ .** Following Yakovlev et al. (2006) we consider only the  $^{12}\text{C}(^1\text{H}, \gamma)^{13}\text{N}$  reaction, activated by the traces of hydrogen left over by the previous phases and still present in the WD. This is one of the three starting reactions that ignite the CNO-cycle, which however cannot be completed, owing to the extremely low abundances of the intermediate elements. This reaction has a  $Q$ -value of 1.94 MeV compared to the 25.02 MeV when the cycle is completed, releasing a factor of 12.5 less energy. The nuclear energy release, the ion internal energy, and the comparison luminosity are all expressed per unit volume of the WD. The volume is calculated from the luminosity and effective temperature of the WD along its cooling sequence. All quantities are provided by Althaus & Benvenuto (1997, 1998) and Renedo et al. (2010).

The temporal evolution of the WD luminosity (red dotted line), nuclear energy release (blue solid line) and thermal energy of the ions (magenta dashed line) are shown in Fig. 11. Since the ion internal energy is derived here from simple expressions, neglecting the effect of degenerate electrons and the variation of the degrees of freedom in the crystal lattice at very low temperatures, we do not extend it to very high densities or low temperatures, characteristic of very old ages. First of all, we notice that the abundance  $X_H$  of the residual hydrogen cannot exceed  $10^{-21}$ , otherwise the nuclear energy release by the sole  $^{12}\text{C}(^1\text{H}, \gamma)^{13}\text{N}$  reaction during the initial stages of WD cooling is comparable to or even exceeds the total luminosity, thus bringing the WD to a risky regime at which a nuclear runaway may start. See also (Renedo et al. 2010) for the energy production by the surface CNO during the same phase. We will see below that the upper limit to  $X_H$  to avoid early nuclear runaway changes with the WD mass,

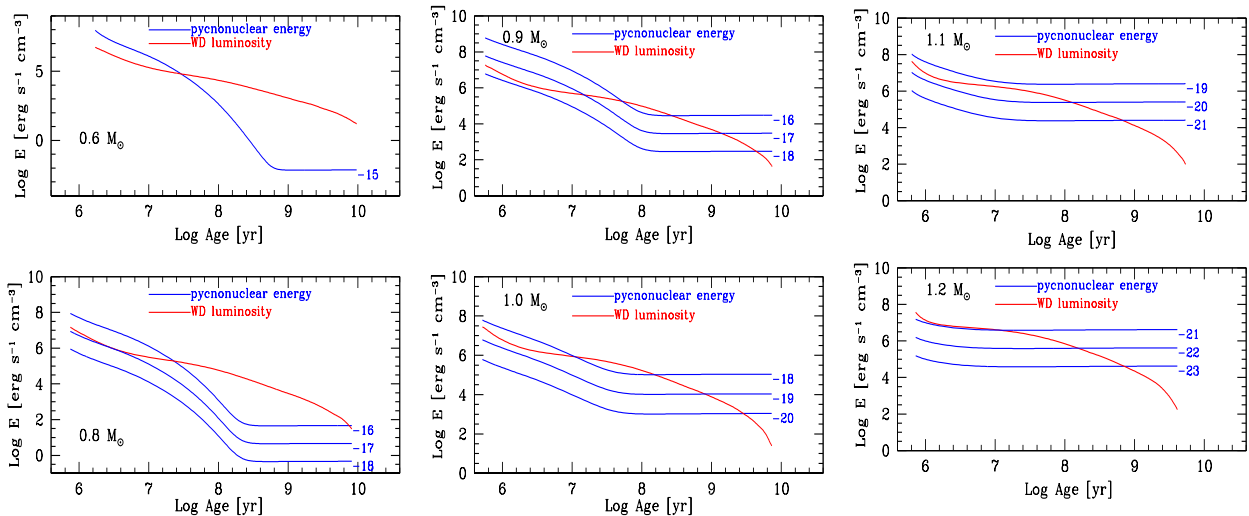


**Figure 12.** Energy rates per unit volume produced by hydrogen impurities with different abundances of  $X_H$  as indicated for WD of different mass. The reaction on display is the  $^{12}\text{C}(^1\text{H}, \gamma)^{13}\text{N}$  according to Yakovlev et al. (2006). The luminosity is in the units as the energy generation.

**Table 7.** Logarithm of the age in yr at which the energy generation ( $\epsilon/V$ ) by the nuclear reaction  $^{12}\text{C}(^1\text{H}, \gamma)^{13}\text{N}$  in  $\text{erg cm}^{-3} \text{s}^{-1}$  crosses the WD luminosity in  $\text{erg cm}^{-3} \text{s}^{-1}$  for different  $M_{WD}$  in  $M_\odot$  and hydrogen abundances  $X_H$ . Ages in *italic* corresponds to very early intersections of the two curves when the temperature is very high and neutrino cooling is very efficient. In these cases, the nuclear energy is most likely carried away and radiated by the star. The other ages in roman correspond to cases in which the energy produced by nuclear reactions could be trapped inside the WD because the energy production by nuclear reactions overwhelms the luminosity and neutrinos have become much less efficient in removing the energy. The luminosities and radii (volumes) of the WDs are from the cooling sequences of Althaus & Benvenuto (1997, 1998).

$M_{WD}$	$\log X_H$								
	-15	-16	-17	-18	-19	-20	-21	-22	-23
0.6	<i>7.5</i>								
0.8		7.4; 9.8	6.5; >10	>10					
0.9		7.6; 8.4	7.2; 9.2	9.8					
1.0				7.0; 8.2	8.8	9.6			
1.1						8.2	8.8		
1.2							7.0	8.2	8.9

it increases at decreasing mass. Incidentally, this constraint may be a way of estimating and calibrating the maximum content of residual hydrogen in a CO-WD.

As cooling proceeds, the energy generation by nuclear reactions in the thermally-enhanced regime decreases and the light contaminants do not have any effect until the pure pycno-nuclear channel begins. In the case of the  $1.2 M_\odot$  star with the hydrogen abundance of  $X_H = 10^{-22}$ , the nuclear energy production exceeds the luminosity at the age of about  $2.5 \times 10^8$  as shown in Fig. 11.  $X_H$  greater than the above value would lead the WD to intersect the luminosity curve during the thermally enhanced phase, i.e. soon after (or shortly later) the formation of the WD itself (a possibility that cannot be firmly excluded and is temporarily left aside, see below).

**Exploring the solution space.** Since the abundances  $X_H$  cannot be assessed a priori, it is safe to consider them as free parameters whose values fall within a plausible range bounded by (a) the maximum value above which the energy production exceeds the WD luminosity during the early stages of the thermally enhanced regime, (b) the lower value below which the energy production equals the WD luminos-

ity at ages older than the age of the Universe. This grid of possible solutions is shown in the various panels of Fig. 12 and the corresponding ages of intersection are listed in Table 7 as function of the WD mass and  $X_H$ . It is worth noting here that intersections occurring during the earliest stages of the cooling sequences are unlikely because cooling by neutrinos is very efficient so that a release of nuclear energy per unit volume and time exceeding the luminosity per unit volume does not trigger any potential instability but simply the energy excess is carried out by radiation and neutrinos. In contrast, the intersections occurring at later stages when the pycno-nuclear regime is already in place and neutrino cooling is over are much more interesting because they can potentially lead to unstable situations.

As expected, at given  $M_{WD}$  the intersection occurs later with decreasing  $X_H$ . For values lower than those indicated, the intersection occur at ages much older than the current age of the Universe (and thus of little interest here). We note that the intersection occurs at lower and lower abundances and younger ages with increasing WD mass. In fact, the luminosity per unit volume (evaluated at the typical age of  $10^9$  yr) increases by a factor of ten from the 0.8 to the

1.2  $M_{\odot}$  WD. Also the central and the mean density of a WD increase with the mass, and so does the efficiency of the pycno-nuclear reactions. Consequently, the values of  $X_{\text{H}}$  for which the intersection may occur within the age of the Universe systematically decrease with increasing WD mass:  $X_{\text{H}} \simeq 10^{-18}$  for the 0.8  $M_{\odot}$  star and  $X_{\text{H}} \simeq 10^{-23}$  for the 1.2  $M_{\odot}$ .

Finally, we note that the systematic decrease of the "permitted" values of  $X_{\text{H}}$  at increasing WD mass is compatible with the past thermal history of the progenitor star. In fact, the mean temperature in a low mass progenitor is lower than the mean temperature in a more massive one, clearly having effects on nuclear burning. For this reason it is tempting to suggest that  $X_{\text{H}}$  decreases with increasing WD mass.

Concluding this section, we remind the reader that the rates of energy generation as function of age have been calculated at constant  $X_{\text{H}}$  and  $X_{\text{C}}$ . In reality,  $X_{\text{H}}$  (and  $X_{\text{C}}$ ) should decrease with time. Therefore a real WD should move along a path in the panel corresponding to its mass gradually shifting to lines of decreasing  $X_{\text{H}}$ . Consequently, the age at which the liberated energy would equal the luminosity cannot be exactly determined without the aid of real models of WD stars including the energy generated by the reactions between contaminants and the carbon (oxygen) nuclei. The ages reported in Table 7 are merely indicative of the expected trend.

## 7.2 To be, or not to be: that is the question (William Shakespeare, Hamlet 3/1)

Adapting Hamlet's famous soliloquy to our contest, the question is whether or not WDs containing traces of light elements (hydrogen in the case we have considered) during cooling produce enough nuclear energy via the  ${}^1\text{H} + {}^{12}\text{C}$  reaction to balance and exceed the WD luminosity. A fraction of the energy would be kept inside the WD creating the physical conditions for C+C-burning, and likely initiating a nuclear runaway followed by explosion.

### 7.2.1 A Fuse for C-ignition

The condition  $\langle \epsilon \rangle \geq L_{\text{WD}}/V$  does not necessarily imply that C-burning is started by the [H + C] reaction and, by proceeding toward C-deflagration (or C-detonation), cause the explosion of the WD. When the energy-luminosity condition occurs in late cooling stages, i.e. when neutrino production does not occur, it only implies that part of the energy can be trapped in the star. For the nuclear runaway a mechanism must provide the threshold energy for carbon-carbon ignition.

According to Nomoto (1982b,a) and Kitamura (2000), the condition to ignite the Carbon-Carbon reaction over a wide range of temperatures ( $10^7 - 10^9$  K) and densities ( $10^8 - 10^{10}$  g cm $^{-3}$ ) in dense matter is  $R_{\text{CC}} \times Q_{\text{CC}}/\rho = 10^{-5}$  W g $^{-1} \equiv 10^2$  erg g $^{-1}$  s $^{-1}$  where  $R_{\text{CC}}$  is the reaction rate (see Sect.3 above) and  $Q_{\text{CC}}$  is the energy released per reaction ( $Q_{\text{CC}} = 13.931$  MeV). This condition is hardly reached via the sole [H+C]-reaction in presence of very low abundances of hydrogen. We suggest that in the physical situation of the WD interiors, in which  $\Gamma > 1$  is soon reached by

cooling and the nuclear burning occurs in regimes from thermally enhanced to pure pycno-nuclear, the threshold limit for C+C-ignition is reached in a different way.

**Elementary burning cells.** Let us start considering a single  ${}^1\text{H} + {}^{12}\text{C}$  reaction. It occurs in a medium in which the carbon and oxygen nuclei are already in liquid, partially crystallized or even fully crystallized conditions, and therefore have reduced their mobility. Consequently, the energy deposited by this reaction will preferentially be given to the neighbouring nuclei, and then shared with a wider environment by conduction and radiation with opacities  $\kappa_{\text{c}}$  and  $\kappa_{\text{r}}$ , respectively, and total opacity  $\kappa = \frac{\kappa_{\text{c}} \times \kappa_{\text{r}}}{\kappa_{\text{c}} + \kappa_{\text{r}}}$ . In the physical conditions of WDs, thermal conduction dominates over radiative transport (see the results of detailed calculations described by Iben 2013a,b, and references therein), therefore  $\kappa \simeq \kappa_{\text{c}}$ . For the purposes of this study we adopt the analytic fits of Iben (1968, 1975) of the numerical conductive opacities by Hubbard & Lampe (1969) and Canuto (1970). The associated mean free path of thermal conduction is

$$\lambda = \frac{1}{\kappa \rho} \quad (75)$$

Both  $\kappa_{\text{c}}$  and  $\lambda$  vary significantly with the temperature and density and in turn with the evolutionary stage and mass of the WD. Looking at the case of the 0.9  $M_{\odot}$  WD, the conductive opacity in the centre varies from  $4 \times 10^{-3}$  cm $^2$  g $^{-1}$  at the beginning ( $T_{\text{c}} \simeq 8 \times 10^7$  K,  $\rho_{\text{c}} \simeq 1.6 \times 10^7$  g cm $^{-3}$ ) to about  $3 \times 10^{-8}$  at the end ( $T_{\text{c}} \simeq 5 \times 10^5$  K,  $\rho_{\text{c}} \simeq 1.8 \times 10^7$  g cm $^{-3}$ ) of the cooling sequence. The mean free path of the energy transportation is of the order of  $\lambda \simeq 4.5 \times 10^{-4}$  cm and 16.7 cm, respectively. Furthermore, within a WD of given mass, the conductive opacity  $\kappa_{\text{c}}$  increases from the centre to the surface and the mean free path does the opposite. In Fig. 13 we show the run of the central value of the conductive opacity along the cooling sequences for all the WD models to our disposal (left panel) and limited to the case of the 1  $M_{\odot}$  the variation of  $\kappa_{\text{c}}$  from the centre to the surface for three selected models characterized by their central temperature (right panel). However, since the nuclear energy by the [H+C]-reaction is expected to occur within a central sphere of rather small dimensions, in the analysis below we may approximate the mean effective conductive opacity of a WD to its central value. In any case, the mean free path of conduction is much longer than the interionic distance  $a_{ij}$  which varies from  $8 \times 10^{-9}$  to  $2 \times 10^{-9}$  cm from a WD of 0.6  $M_{\odot}$  to a WD of 1.2  $M_{\odot}$ .

In this scenario, it is plausible to conceive that most of the energy emitted by a single [H+C]-reaction is acquired by the nuclei contained in a small volume, which is approximated to a cube of edge  $\lambda$  centered on the H-nucleus. In the volume  $\lambda^3$  there are  $N_{\text{C}}$  nuclei of carbon and  $N_{\text{O}}$  nuclei of oxygen. This volume is named the *elementary burning cell*. The ratio  $(\lambda/a_{ij})^3$  indicates of the total number of nuclei inside the cell,  $N_{\text{C}} + N_{\text{O}} \equiv 2 \times N_{\text{C}} = (\lambda/a_{ij})^3$ . Depending on the local values of total opacity and density, we estimate  $N_{\text{C}} \simeq 10^{16} - 10^{19}$ . The  $Q_{\text{HC}} \simeq 1.95$  Mev of a single [H+C]-reaction is the source of energy for the nuclei of carbon and oxygen in the cell. The amount of energy to be shared per unit mass in the cell  $\lambda^3$  is

$$\frac{Q}{\rho \lambda^3} \quad (76)$$

where  $Q_{\text{HC}}$  is expressed in erg and  $\rho \lambda^3$  is the mass of the cell.

**Table 8.** Columns (1) through (11) are: (1)  $M_{WD}$  the WD mass in  $M_{\odot}$ ; (2)  $\log X_H$ ; (3)  $\log Age$  in yrs; (4) the central density  $\rho_c$  in  $g\text{ cm}^{-3}$ ; (5) the central temperature  $T_c$  in K; (6) the reaction rate  $R_{H,C}$  in  $n\text{ s}^{-1}\text{ cm}^{-3}$ ; (7) the energy generation rate  $\epsilon$  in  $\text{erg cm}^{-3}\text{ s}^{-1}$ ; (8) the energy generation rate  $\frac{\epsilon\lambda}{\rho}$  per gram in the elementary volume  $\lambda^3$  in  $\text{erg g}^{-1}\text{ s}^{-1}$ ; (9) the energy difference  $\Delta E = \text{WD luminosity per unit volume} - \text{nuclear energy generation per unit volume}$  in  $\text{erg cm}^{-3}\text{ s}^{-1}$ . The negative sign in brackets and in front of  $|\Delta E|$  means that  $\Delta E$  is negative; (10) the time in sec required to process all [H+C]-reactions in a gram of matter; (11) the total opacity  $\kappa \simeq \kappa_c$  in  $\text{cm}^2\text{ g}^{-1}$ . The mean free path of thermal conduction is  $\lambda = 1/(\rho\kappa)$ . The reaction and energy generation rates per unit mass and time are  $R_{H,C}/\rho$  and  $\epsilon/\rho$ , respectively. The Q-value of the [H+C]-reaction is  $3.108 \times 10^{-6}\text{ erg/reaction}$ . The threshold value for C-burning  $\epsilon_{CC} = 10^2\text{ erg g}^{-1}\text{ s}^{-1}$ . Finally,  $\frac{\epsilon\lambda}{\rho}$  is expected to be equal to  $\epsilon_{CC}$ .

$M_{WD}$	$\log X_H$	$\log Age$	$\log \rho_c$	$\log T_c$	$\log R_{H,C}$	$\log \epsilon$	$\log \frac{\epsilon\lambda}{\rho}$	$\log  \Delta E $	$\log Time$	$\log \kappa$
0.6	-14	8.35177	6.55997	7.19447	7.10141	1.59388	1.92175	(-)3.94112	7.95889	-4.33077
0.6	-15	8.24095	6.55871	7.25346	6.79210	1.28457	1.99387	(-)4.07929	7.25004	-4.20843
0.6	-16	8.13146	6.55737	7.30867	6.43479	0.92725	1.99437	(-)4.20756	6.59058	-4.09341
0.6	-17	8.02755	6.55603	7.35761	5.99829	0.49075	1.87563	(-)4.31829	6.01263	-3.99095
0.6	-18	7.89861	6.55429	7.41307	5.62932	0.12179	1.86722	(-)4.44405	5.36593	-3.87426
0.6	-19	7.75130	6.55223	7.47019	5.26896	-0.23858	1.87873	(-)4.57408	4.71112	-3.75329
0.6	-20	7.56597	6.54952	7.53408	4.96728	-0.54026	1.99383	(-)4.72370	3.99713	-3.61688
0.6	-21	7.38734	6.54662	7.58990	4.56002	-0.94752	1.95181	(-)4.86916	3.39188	-3.49641
0.6	-22	7.16977	6.54240	7.65074	4.18331	-1.32423	1.97544	(-)5.06910	2.75617	-3.36288
0.8	-14	8.52201	7.02594	7.09378	9.17690	3.66936	1.97868	(-)3.93600	6.45311	-5.27969
0.8	-15	8.31731	7.02427	7.21050	8.39026	2.88273	1.95233	(-)4.37791	6.19206	-5.04049
0.8	-16	8.18340	7.02304	7.28099	7.81197	2.30443	1.86132	(-)4.55444	5.71492	-4.89531
0.8	-17	8.03733	7.02158	7.35189	7.42634	1.91880	1.95147	(-)4.72227	5.06044	-4.74862
0.8	-18	7.89409	7.02008	7.41467	7.02794	1.52040	1.96527	(-)4.86833	4.43377	-4.61807
0.8	-19	7.74364	7.01846	7.47349	6.60320	1.09566	1.92477	(-)5.00203	3.83823	-4.49514
0.8	-20	7.56920	7.01658	7.53337	6.18817	0.68063	1.90075	(-)5.13687	3.23409	-4.36931
0.8	-21	7.35847	7.01436	7.59534	5.78730	0.27976	1.90494	(-)5.27617	2.61641	-4.23826
0.8	-22	7.11746	7.01181	7.65611	5.36457	-0.14296	1.87995	(-)5.41917	2.02231	-4.10874
0.9	-14	9.07445	7.26987	6.74175	11.97203	6.46449	1.96448	(+)6.46393	3.94219	-6.36532
0.9	-15	8.83613	7.26875	6.90389	10.96806	5.46052	1.94121	(+)5.44860	3.94616	-6.03731
0.9	-16	8.54620	7.26701	7.07901	9.96173	4.45419	1.99767	(+)3.94001	3.95236	-5.68135
0.9	-17	8.27756	7.26491	7.23405	8.96598	3.45844	1.94997	(-)4.62444	3.94478	-5.36434
0.9	-18	8.01843	7.26247	7.36559	8.10553	2.59800	1.93500	(-)4.95998	3.76529	-5.09338
0.9	-19	7.81745	7.26038	7.45365	7.49842	1.99088	1.94260	(-)5.16469	3.29955	-4.91068
0.9	-20	7.63707	7.25849	7.52097	6.98654	1.47901	1.89308	(-)5.31693	2.76507	-4.77012
0.9	-21	7.42745	7.25636	7.58690	6.53473	1.02719	1.88136	(-)5.46365	2.18577	-4.63166
0.9	-22	7.17789	7.25393	7.65287	6.10282	0.59528	1.88488	(-)5.60437	1.59335	-4.49220
1.0	-14	9.39692	7.53170	6.41961	14.54245	9.03491	1.92506	(+)9.03491	1.65015	-7.40431
1.0	-15	9.24047	7.53132	6.58673	13.54068	8.03315	1.92948	(+)8.03313	1.65191	-7.06854
1.0	-16	9.04733	7.53067	6.75247	12.53808	7.03054	1.92630	(+)7.03028	1.65451	-6.73474
1.0	-17	8.80496	7.52952	6.92807	11.53392	6.02639	1.98335	(+)6.02026	1.65867	-6.37987
1.0	-18	8.52880	7.52782	7.09582	10.52770	5.02016	1.99405	(+)4.84002	1.66488	-6.03919
1.0	-19	8.26222	7.52570	7.25066	9.52116	4.01363	1.92983	(-)4.85314	1.67121	-5.72304
1.0	-20	7.93496	7.52246	7.41753	8.52990	3.02236	1.96429	(-)5.29860	1.65732	-5.37960
1.0	-21	7.62916	7.51914	7.54204	7.64720	2.13966	1.88934	(-)5.58367	1.49859	-5.12084
1.0	-22	7.31205	7.51584	7.64026	7.01341	1.50588	1.94940	(-)5.79626	1.04672	-4.91482
1.1	-14	9.54505	7.82986	6.14979	16.91043	11.40289	1.98658	(+)11.40289	-0.44007	-8.37871
1.1	-15	9.44801	7.82976	6.31254	15.90966	10.40213	1.96387	(+)10.40213	-0.43931	-8.05259
1.1	-16	9.32710	7.82956	6.47463	14.90856	9.40103	1.93754	(+)9.40103	-0.43821	-7.72746
1.1	-17	9.16675	7.82915	6.64704	13.90679	8.39926	1.97362	(+)8.39925	-0.43644	-7.38110
1.1	-18	8.97695	7.82848	6.80741	12.90427	7.39673	1.93788	(+)7.39649	-0.43391	-7.05817
1.1	-19	8.74844	7.82733	6.97449	11.90026	6.39273	1.94316	(+)6.38691	-0.42991	-6.72059
1.1	-20	8.46042	7.82544	7.14373	10.89416	5.38663	1.96240	(+)5.21465	-0.42381	-6.37693
1.1	-21	8.17092	7.82287	7.31018	9.88766	4.38012	1.96812	(-)5.23897	-0.41736	-6.03697
1.1	-22	7.83702	7.81916	7.47749	8.88169	3.37415	1.98576	(-)5.67932	-0.41220	-5.69232
1.2	-14	9.54748	8.19896	5.90131	19.12970	13.62216	1.99528	(+)13.62216	-2.38222	-9.39229
1.2	-15	9.48817	8.19894	6.06513	18.12936	12.62183	1.97860	(+)12.62183	-2.38189	-9.06438
1.2	-16	9.41359	8.19889	6.22851	17.12885	11.62132	1.95941	(+)11.62132	-2.38138	-8.73723
1.2	-17	9.32198	8.19879	6.39158	16.12812	10.62058	1.93851	(+)10.62058	-2.38064	-8.41051
1.2	-18	9.19360	8.19855	6.56513	15.12693	9.61939	1.98084	(+)9.61939	-2.37945	-8.06243
1.2	-19	9.03909	8.19810	6.72674	14.12516	8.61762	1.95172	(+)8.61760	-2.37768	-7.73777
1.2	-20	8.83129	8.19725	6.89917	13.12217	7.61464	1.98801	(+)7.61417	-2.37470	-7.39049
1.2	-21	8.60565	8.19587	7.06372	12.11783	6.61030	1.97738	(+)6.59886	-2.37036	-7.05788
1.2	-22	8.34100	8.19411	7.22991	11.11314	5.60561	1.97863	(+)5.19378	-2.36567	-6.72080



**Figure 13. Left Panel:** The run of the central conductive opacity  $\kappa_c$  (in  $\text{cm}^2 \text{g}^{-1}$ ) as a function of the central temperature  $T_c$  along the cooling sequence in WDs of different mass as indicated. **Right Panel:** the run of the conductive opacity from the center to the surface in the  $1.0 M_\odot$  WD for three different values of the central temperature  $T_c$ . The other masses have a similar trend. The cooling sequences and models of internal structure are from Althaus & Benvenuto (1997, 1998).

The above ratio for typical values of density ( $10^8 \text{ g cm}^{-3}$ ) and mean free path ( $4 \times 10^{-4} \text{ cm}$ ) turns to be in the range 0.01 to 0.001. We multiply this quantity by the total rate  $R$  (in  $\text{N cm}^{-3} \text{s}^{-1}$ ) of the [H+C]-reactions to obtain the total energy to be shared. This energy is mostly used to heat the carbon and oxygen nuclei in the elementary cell.

The above limit for C-ignition of about  $10^2 \text{ erg g}^{-1} \text{s}^{-1}$  has to be applied to the quantity of carbon in the elementary burning cell (the dimensions of which already take conduction into account).

In this model in which the WD medium is populated by many elementary cells around the hydrogen nuclei, the condition for C-ignition must be suitably scaled and applied to the environment of the cells. We define the quantities

$$\epsilon_\lambda = \epsilon \times \frac{1 \text{ cm}^3}{\lambda^3} \quad (77)$$

$$\epsilon_{g,\lambda} = \epsilon_g \times \frac{1 \text{ cm}^3}{\lambda^3} = \frac{\epsilon_\lambda}{\rho} \quad (78)$$

where  $\epsilon$  is the energy per  $\text{cm}^3$ , and  $\epsilon_\lambda$  the energy per  $\text{cm}^3$  in the volume  $\lambda^3$ , and  $\epsilon_{g,\lambda}$  the energy per gram in the same volume. We show that the energy deposited by a single [H+C]-reaction, when trapped into the elementary cell, is sufficient to heat and finally ignite the C-nuclei inside the cell (see the entries in Table 8).

Because of the above considerations, along the evolutionary sequence of a WD of assigned mass we calculate the reaction rate and associated energy production rate of the [H+C]-reaction both per unit volume and unit mass (expressed in  $\text{N cm}^{-3} \text{s}^{-1}$ ,  $\text{erg cm}^{-3} \text{s}^{-1}$ ,  $\text{N g}^{-1} \text{s}^{-1}$  and  $\text{erg g}^{-1} \text{s}^{-1}$ , as appropriate) and also the quantity  $\epsilon_\lambda/\rho$  (the energy generated in the elementary volume  $\lambda^3$  sampled by the mean free path of conductive energy transport). We remind the reader that the above reaction rate depends also on  $X_H$  (here considered as a free parameter).

**Criterion for initiating a nuclear runaway.** Given

these premises, along the cooling sequence of a WD of a given mass we identify the time at which the energy input by the [H+C]-reaction to the elementary cell,  $[\epsilon_\lambda/\rho]$  falls below the threshold value for C-ignition  $\epsilon_{CC} = 100 \text{ erg g}^{-1} \text{s}^{-1}$ . Since we are moving along a cooling sequence from high to low values of  $T_c$  (the density remains nearly constant), during all previous stages, the energy  $\epsilon_\lambda/\rho$  is always above the threshold value. Along the same cooling sequence we search the time at which the condition  $\langle \epsilon \rangle \geq L_{WD}/V$  is verified, thus initiating the energy trapping. *The two conditions must be simultaneously satisfied to start C-burning in a situation of energy trapping.*

The results of these calculations are summarized in Table 8 which for each value of  $X_H$  lists a few key quantities at the stage at which the nuclear energy generation by the  ${}^1\text{H}+{}^{12}\text{C}$  reaction satisfies the conditions  $\langle \epsilon \rangle \geq L_{WD}/V$  and  $\epsilon_\lambda/\rho \leq 10^2 \text{ erg g}^{-1} \text{s}^{-1}$ . The physical quantities listed in Table 8 are: (1) the WD mass  $M_{WD}$  in solar units; (2) the hydrogen abundance  $\log X_H$ ; (3) the logarithm of the age in years at which for the first time the elementary cell does not reach the conditions for C+C-ignition; (4)-(5) the corresponding central density and temperature  $\rho_c$  in  $\text{g cm}^{-3}$  and  $T_c$  in K; (6) the reaction rate per unit volume and time  $R_{H,C}$  in  $\text{cm}^{-3} \text{s}^{-1}$ ; (7) the energy generation rate per unit volume and time  $\epsilon$  in  $\text{erg cm}^{-3} \text{s}^{-1}$ ; (8) the energy generation rate per unit mass and time within the elementary cell of volume  $\lambda^3$   $\frac{\epsilon_\lambda}{\rho}$  in  $\text{erg g}^{-1} \text{s}^{-1}$ ; (9) the difference  $\Delta E = \langle \epsilon \rangle - L_{WD}/V$  in  $\text{erg cm}^{-3} \text{s}^{-1}$ . To display  $\Delta E$  on a logarithmic scale, we take the absolute value adding a negative (positive) sign when the difference is negative (positive). The positive sign is for the nuclear energy generation exceeding the luminosity; (10) logarithm of the time in s required to process all [H+C]-reactions in a gram of matter; and finally (11) the total opacity  $\kappa \simeq \kappa_c$  in  $\text{cm}^2 \text{g}^{-1}$ .

At this stage of the analysis, we use three parameters: the abundance  $X_H$ , the age ( $\tau_1$ ) at which the nuclear energy generation rate per unit volume exceeds the WD luminosity

per unit volume (see the intersections shown in Fig 12 and the entries of Table 7), and the age  $\tau_2$  at which  $\epsilon_\lambda/\rho$  falls below  $\epsilon_{CC}$  in the elemental burning cell for the first time. The abundance  $X_H$  can be further constrained by imposing that the nuclear rate per unit volume during the first cooling stages remains smaller than the WD luminosity per unit volume. This avoids very early ignition, which is unlikely for the majority of WDs since we do observe most of them to live and cool for a long time. This means that for each WD mass there is an upper limit of  $X_H$  which decreases with increasing WD mass as already suggested by the intersections in Fig. 12.

An explosion may only occur with  $\tau_1 \leq \tau_2$ , as illustrated in Fig. 14 where the WD luminosity per unit volume, the energy per unit volume produced by the [H+C]-reaction for two reasonable values of  $X_H$ , the energy  $\epsilon_\lambda/\rho$  for the same values of  $X_H$ , and finally the threshold value  $\epsilon_{CC}$ , all of them as function of time and on the same logarithmic scale. Looking at the panels of Fig. 14, the condition can be met by WDs with mass 0.9, 1.0, 1.1 and 1.2  $M_\odot$  whereas it is missed by WDs with mass smaller than 0.8  $M_\odot$ . In the latter stars, the energy production falls below  $\epsilon_{CC}$  at ages  $\tau_2 \ll \tau_1$ . The condition could be met, however, by a 0.85  $M_\odot$  WD, and finally the 0.8  $M_\odot$  WD is border line.

**Global estimates of energy production.** In order to better highlight the above numerical results, we present some analytical estimates of (i) the total energy released by the [H+C]-reactions, (ii) the fraction of this energy released inside an elementary cell, to assess whether it is sufficient to increase the temperature of C-nuclei contained in the cell to the threshold value for C-burning, and (iii) the total amount of energy produced by C-burning in the whole WD:

(i) [H+C]-burning. In a WD there are  $X_H \times M_{WD} \times M_\odot$  (the  $M_{WD}$  mass is in solar units) grams of hydrogen or equivalently a total number of hydrogen nuclei

$$N_H = \frac{X_H \times M_{WD} \times M_\odot}{A_H \times m_u}$$

approximating  $M_{WD} = 1 M_\odot$ ,  $M_\odot = 1.989 \times 10^{33}$  g and using  $A_H = 1$  we obtain

$$N_H = 1.19 \times 10^{57} \times X_H$$

Adopting for  $X_H$  a typical value of  $10^{-20}$  and considering the energy generated by each [H+C]-reaction, i.e.  $3.12 \times 10^{-6}$  erg, we obtain a total energy release of  $E_{[H+C]} = 10^{31}$  erg. For a typical WD volume of  $\simeq 5.2 \times 10^{26} \text{ cm}^3$  the nuclear energy per unit volume is about  $2 \times 10^5$ , much higher than the WD luminosity per unit volume  $\simeq 8 \times 10^3$ .

(ii) [C+C]-ignition. In order to verify whether the energy deposited by the [H+C]-reactions in the elementary cell may increase the temperature of the latter to that of C-ignition ( $\simeq 0.6 - 0.7 \times 10^9$  K), we start from Nomoto (1982b,a); Kitamura (2000) condition for C-ignition, the cell acquires the energy  $\frac{\epsilon_\lambda}{\rho} \times \left(\frac{\rho}{\langle R_{ij} \rangle \times \lambda^3}\right)$ . This energy goes into the total energy of the particles in the elemental cell, i.e.  $\frac{3}{2} k_B T \times N_V$ , where  $N_V$  is the total number of particles in the cell, i.e. the equation

$$\frac{\epsilon_\lambda}{\rho} \times \left(\frac{\rho}{\langle R_{ij} \rangle \times \lambda^3}\right) = \frac{3}{2} k_B T N_V \quad (79)$$

is verified. According to its definition,  $\epsilon_\lambda/\rho \equiv \epsilon_{CC} \simeq 10^2 \text{ erg g}^{-1} \text{ s}^{-1}$  and  $\langle R_{ij} \rangle = \langle \epsilon_{ij} \rangle / Q_{HC}$ . In addition, each elementary cell contains only one nucleus of hydrogen, so in a cell the [H+C]-reaction occurs only once and therefore the cell acquires only this specific amount of energy. Consequently,

$$T = \frac{2}{3} \epsilon_{CC} \times \left(\frac{A_C \times m_u}{k_B \times \lambda^3}\right) \times \left(\frac{1}{\langle R_{ij} \rangle \times \lambda^3}\right) \times \eta \quad (80)$$

where  $N_V$  has been replaced by  $(\rho \times \lambda^3)/(A_C \times m_u)$ ,  $A_C = 12$ , and all other symbols have their usual meaning. For typical values of  $\lambda \simeq 10^{-4} - 10^{-5}$  and  $\langle R_{ij} \rangle \simeq 10^{10} - 10^{11}$ , we estimate a temperature in the range  $10^8 - 10^{14}$  K. In the above equation, we have also introduced the  $\eta$  parameter to take into account that part of the energy may escape from the cell. While the lower limit temperature is below the threshold for C-burning, the temperature at upper limit would require  $\eta \simeq 10^{-4}$ . This means that a small adjustment of the parameters and/or the effective energy acquired by the cell would yield the right temperature. The numerical calculations show that the ignition temperature is reached all cases we have considered.

(iii) [C+C]-burning. Once C-burning is ignited in the elementary cells, how much energy is released by burning all the carbon nuclei contained in the cells? The C+C reaction has a  $Q_{CC}$ -value of 13.93 Mev ( $2.23 \times 10^{-5}$  erg). The number of C pairs in a cell is about  $N_C/2$  (for solid medium). With the aid of the reaction rates of Yakovlev et al. (2006) (see Sect.3 above), we evaluate the rate ( $\text{N cm}^{-3} \text{ s}^{-1}$ ) at the temperature of  $6 \times 10^8$  K and density of  $10^8 \text{ g cm}^{-3}$ . The rate is about  $2.15 \times 10^{22} \text{ cm}^{-3} \text{ s}^{-1}$  and the energy generation rate is  $4.8 \times 10^{18} \text{ erg g}^{-1} \text{ s}^{-1}$ . With the above rates, all carbon nuclei in a cell are destroyed in a tiny fraction of a second.

Since the total number of burning cells is equal to the total number of hydrogen nuclei and the total number of [C+C]-reactions per cell is  $N_C/2$ , the total energy release  $E_{C+C}$  is

$$\begin{aligned} E_{C+C} &= 2.23 \times 10^{-5} \times M_\odot \times M_{WD} \times N_0 \times X_H \times \frac{N_C}{2} \\ &= 1.33 \times 10^{52} \times M_{WD} \times X_H \times N_C \end{aligned} \quad (81)$$

where  $M_{WD}$  is in solar units, and  $N_0 = 6.025 \times 10^{23}$  the Avogadro number. For  $X_H = 10^{-20}$ ,  $N_C \simeq 10^{18} - 10^{19}$ , and  $M_{WD} = 1$  the above equation yields  $E_{C+C} \simeq 10^{50} - 10^{51}$  erg. This energy is comparable to or larger than the total gravitational energy of a WD, varying between  $|\Omega| = 5.5 \times 10^{50}$  erg for the  $0.6 \times M_\odot$  to  $|\Omega| = 5.8 \times 10^{51}$  erg for the  $1.2 \times M_\odot$ . Once started, [C+C]-burning will likely cause a thermal runaway followed by the explosion of the star.

**The fuse for C-ignition.** Since in any elemental volume, thanks to the energy released by the [H+C]-reaction the condition for local, mild C-ignition is met, we name this two steps process the "fuse for C-ignition". Most likely, once the fuse is activated, the additional release of energy by C-burning makes it even stronger, propagating it to neighbouring regions, and activating complete C-burning that gradually moves into the thermally driven regime.



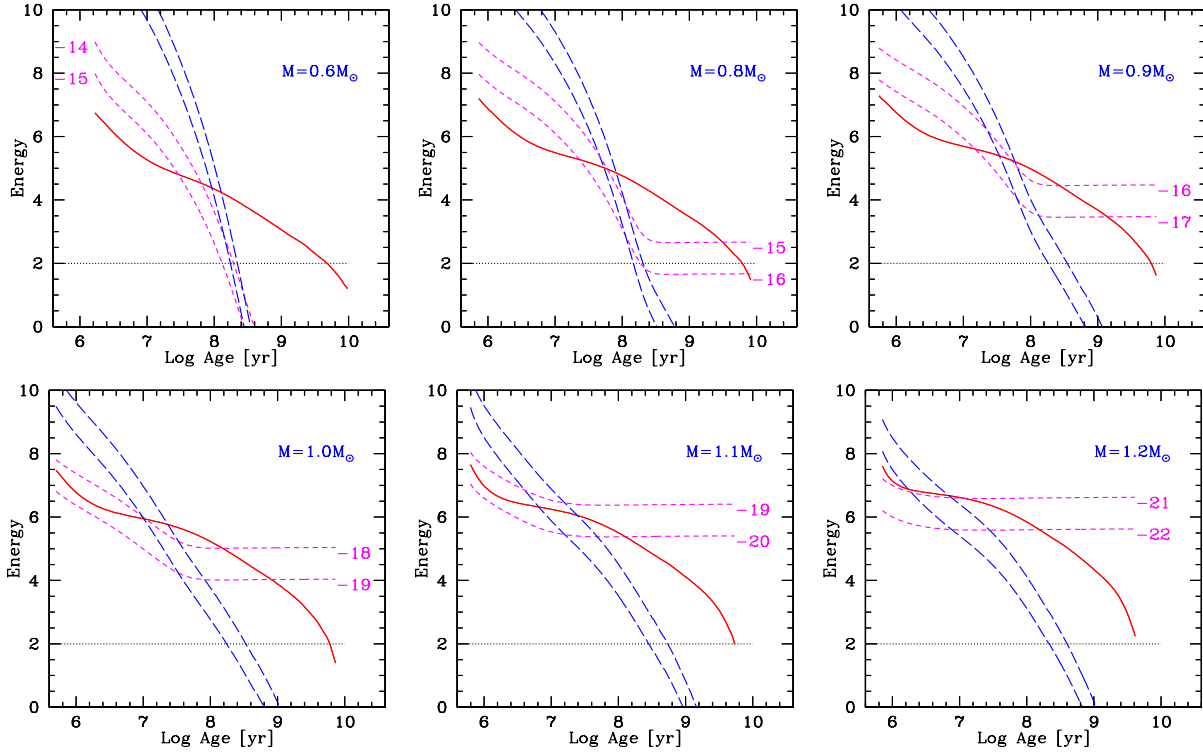


**Figure 14.** The WD luminosity per unit volume (thick red solid line), the energy per unit volume produced by the [H+C]-reaction for two reasonable values of  $X_{\text{H}}$  (the thin, short-dashed magenta lines) that change with the WD mass, the energy  $\epsilon_{\lambda}/\rho$  acquired by a typical burning cell for the same values of  $X_{\text{H}}$  (the thin, long-dashed green lines), and finally the threshold value  $\epsilon_{\text{CC}}$  (the horizontal, dotted black line), all of which are plotted as a function of the age in years. The various energies are plotted on the same logarithmic scale. From left to right, WDs with different masses are displayed, i.e. 0.6, 0.8, 0.9, 1.0, 1.1, and 1.2  $M_{\odot}$  respectively.

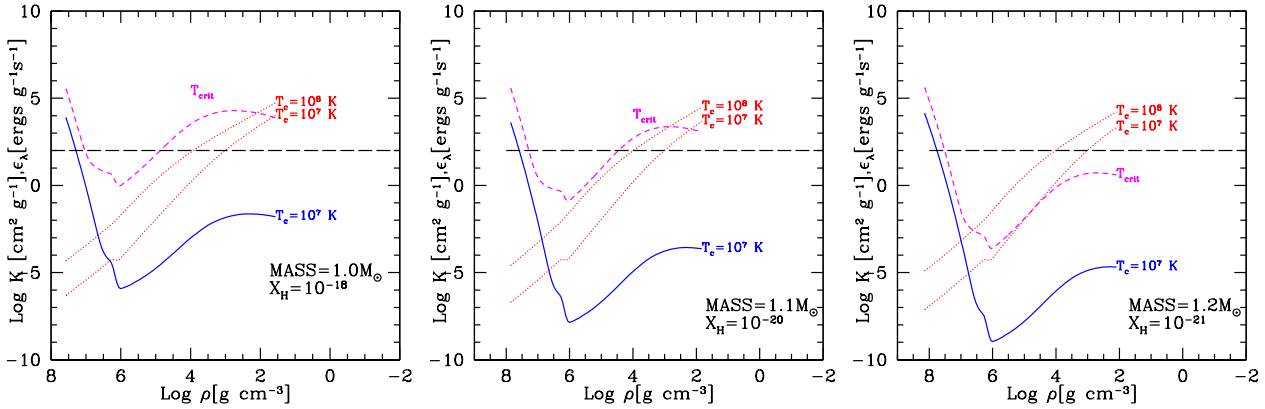


**Figure 15.** The run of the energy  $\epsilon_{\lambda}/\rho$  in  $\text{erg g}^{-1} \text{s}^{-1}$  produced inside an elementary cell by the [H+C]-reaction as a function of radial distance from the centre. The distance from the centre is described by the density decreasing from the center toward the surface. The energy production is presented for two values of the central temperature  $T_c$  (assumed also to be the temperature throughout the WD):  $T_{\text{crit}}$  the value at the stage when  $\epsilon_{\lambda}/\rho$  becomes for the first time  $\leq \epsilon_{\text{CC}} = 10^2 \text{ erg g}^{-1} \text{ s}^{-1}$ , and a lower value  $T_c = 10^7 \text{ K}$  for comparison. The dotted lines show the run of the conductive opacity for two values of  $T_c$  as indicated. All the quantities are plotted on the same logarithmic scale. Two intersections are possible for the curve labelled  $T_{\text{crit}}$  with the horizontal line corresponding to  $\log \epsilon_{\text{CC}} = 2$  in the case of the 1.0 and 1.1  $M_{\odot}$  WDs. The first one is at the center and the second one occurs at  $\log \rho \simeq 5$  and 5.5, for the 1.0 and 1.1  $M_{\odot}$  stars, respectively. Off-center C-ignition is possible. Only the intersection at the center occurs for the 1.2  $M_{\odot}$ . No off-center C-ignition is expected.

**Off-center C-ignition.** The analysis we have made so far relies on the model of elementary cells, based on the central values of conductive opacity, temperature, and density. We have already shown that the conductive opacity and mean free path of thermal transport vary along the radius of a WD (see the right panel of Fig. 13). Therefore it is worth investigating if the energy condition for C-ignition in the elementary cells can be met also in more external regions (off-center ignition). To this aim we show in Fig. 15 the energy production by the [H+C]-reaction as a function of radial distance measured here by the value of local density  $\rho(r)$ . The energy is evaluated adopting the temperature of the models listed in Table 8, shortly indicated here by  $T_{crit}$ , and also the value of  $10^7$  for comparison, and for  $X_H$  the value indicated by the results of Table 8 for each WD mass. This energy production is indicated in Fig. 15 by the heavy solid red line for  $T_{crit}$  and the dashed blue line for  $T = 10^7$  K. Together with this we plot the conductive opacity as a function of  $\rho(r)$  and the two temperatures in question. Finally, we show the threshold energy for C-ignition (horizontal line). All quantities are shown on the same logarithmic scale. The three panels correspond to three values of the WD mass as indicated. The intersection of the threshold value  $\epsilon_{CC}$  and the  $T_{crit}$  curve is possible for the 1.0 and 1.1  $M_\odot$  WDs whereas it is missing for the 1.2  $M_\odot$ . The intersection occurs at the centre (situations that we have already considered) and at some intermediate region ( $\rho \simeq 10^5$  g cm $^{-3}$ ). Off-center ignition is therefore possible.

### 7.2.2 General remarks

To summarize, the main results of our analysis are:

(i) The above reaction always occurs in physical conditions with  $\Gamma_{ij} \geq 1$ , transiting from the third (thermally-enhanced) to the fifth regime (pure pycno) of burning (see Section 3.3). This is well evident looking at the variation of the rate of energy generation per unit time and volume by the [H+C]-reaction as a function of the age (along the cooling sequence). The energy generation rate is according to Yakovlev et al. (2006), eqn. (26), i.e. made of two terms  $R_{ij}^{pyc}(\rho) + \Delta_{ij}(\rho, T)$  whose meaning is straightforward. At high temperatures (early stages of the cooling sequence) the second term dominates and the rate steadily decreases, however past a certain temperature, the first term drives the rate and, since the density in a WD is essentially fixed by the mass and remains nearly constant as long as the mass does not change, the rate levels off. We may picture this by saying that the density driven nuclear regime acts as a wedge to stabilize the otherwise ever decreasing temperature dependent rates.

(ii) In low mass WDs, the third regime is initially more efficient than the fifth regime and the latter overwhelms the former only past a certain age, whereas in high mass WDs the fifth regime always prevails. This trend is due to the increase of central and mean density with the WD mass.

(iii) Depending on  $X_H$  and  $M_{WD}$ , the sum of nuclear energy and ion internal energy can equal the luminosity at any age along the cooling sequence.

(iv) Massive WDs are more sensitive to the instability threshold that can be reached even with very small hydrogen abundances. Therefore the reaction  ${}^1\text{H} + {}^{12}\text{C}$  is easily ignited and a nuclear runaway can be started as soon as massive

WDs are born. For a typical value of  $X_H \simeq 10^{-20}$ , the above situation should occur for  $M_{WD} \geq 1.0$ . Although WDs of this mass are rare, the possibility cannot be discarded and it may be possible to identify such progenitors.

(v) WDs of lower mass, about 0.9  $M_\odot$ , are more stable and encounter the threshold condition only after a certain amount of time has elapsed since their formation (in the present analysis about 1 Gyr). WDs of 0.8  $M_\odot$  are at the borderline, in the sense that the two conditions could be met for  $-14 < X_H \leq -13$ . WDs of about 0.85  $M_\odot$  could be the transition stars. Finally WDs of even lower mass cool down to low temperature without reaching the threshold energy for C-ignition.

(vi) We suggest that a future investigation should address the possible correlation between the WD mass (and its progenitor) and  $X_H$  (or  $X_{\text{He}}$ ), which translates into an additional dependence of the explosion time on the WD mass.

(vii) Finally, the onset of nuclear runaway should be a consequence of the positive gravo-thermal specific heat of a mixture of nuclei and electrons whose equation of state is basically driven by the highly degenerate electrons, see the discussion by Kippenhahn & Weigert (1990) and Mestel (1952b,a).

To conclude, there is an ample range of possibilities for WDs contaminated by the presence of traces of light elements in their interiors to reach the critical stage at which nuclear burning is activated, followed by nuclear runaway and consequent disruption of the star.

This semi-analytical, orders-of-magnitude analysis does not yield more information. Only detailed numerical models can give the correct answer to the Hamlet question.

## 8 CONCLUSIONS

In this paper we investigated the possible effects of impurities on the pycno-nuclear reaction rates in CO-WDs. We reviewed the present-day pycno-nuclear reaction rates, highlighting the peculiarities of each model and the use that has been done until now. We introduced two important modifications in the existing expressions:

i) We extended the Salpeter & van Horn (1969) and Shapiro & Teukolsky (1983) reaction rate, to calculate the variation of the coulombian potential induced by the presence of a lighter ion of hydrogen or helium in an arbitrary node of the C-O ion lattice. Thus we extended the original formulation for pycno-nuclear reaction rates conceived for OCPs to BIMs, including the reactions  ${}^1\text{H} + {}^{12}\text{C}$  and/or  ${}^4\text{He} + {}^{12}\text{C}$ .

ii) We evaluated the displacement of nearby nuclei produced by the presence of impurities of different charge and estimated the change in local density, and applied this to the MHO, Kitamura (2000), and Yakovlev et al. (2006) expressions.

Using the above revision of the theoretical rates, we made a preliminary analysis using the MHO formalism to study the pycno-nuclear reactions between light nuclei (hydrogen or helium) present in extremely low abundances and heavier nuclei like carbon and oxygen, the basic constituents of WDs.

Encouraged by the results obtained with the MHO rates, we used the more sophisticated descriptions of nuclear

reactions in high density environments by Kitamura (2000) and Yakovlev et al. (2006) to explore the effects of impurities of light elements in triggering the above reactions.

The main results of the present study suggest that:

- The presence of hydrogen even in extremely low concentrations (from  $10^{-16}$  to  $10^{-21}$ ) can raise the pycno-nuclear reaction rates in density intervals from  $10^7$  to  $10^8$   $\text{g cm}^{-3}$ . The same is true for helium at somewhat higher threshold densities.

- In the case of hydrogen, the above density interval corresponds to WD masses from  $\simeq 0.85$  to  $1.2M_{\odot}$ , well below the known limit of the Chandrasekhar mass.

- In WDs in this mass range, the energy released by pycno-nuclear reactions like  ${}^1\text{H} + {}^{12}\text{C}$  may trigger the ignition of CC-burning in a two steps process that we have named *the fuse of C-ignition*. The age at which this is expected to occur depends on the WD mass and abundance of residual hydrogen. The fuse-induced C-ignition is likely followed by thermal runaway according to the classical mechanisms.

- Even WDs with masses as low as  $0.85 M_{\odot}$  may experience nuclear runaway.

Our results could in principle radically change not only the current understanding of the structure and evolution of WDs but also imply that single WDs may be progenitors of type Ia SNe. We may have discovered an alternative channel to SNa Ia explosions. In this way we may be able (i) to explain the star formation rate dependence of the SNa Ia rate (e.g., Mannucci et al. 2006); (ii) to provide some clues to interpreting the observational data on the ejected mass distribution of type Ia SNe showing a significant rate of non-Chandrasekhar-mass progenitors of mass as low as  $0.8 M_{\odot}$  (Scalzo et al. 2014); and (iii) to account for the SNe exploding inside Planetary Nebulae (shortly named SNIPs) in alternative to the core-degenerate scenario in which a WD merges with the hot core of an AGB star on a time interval  $\leq 3 \times 10^8$  yr since the WD formation (see Tsebrenko & Soker 2014a,b, for more details ). With our models, a single CO-WD may reach the explosion stage soon after the formation if sufficiently massive ( $\geq 1.0 M_{\odot}$ ) and sufficiently rich in residual hydrogen ( $X_{\text{H}} \simeq 10^{-19} - 10^{-20}$ ). The expected time delay after formation can be as low as about a few ten of thousand years.

Therefore, before proceeding further it is mandatory to remind the reader of the limitations of the present approach.

- Prior to any other consideration, it is worth recalling that the success of the proposed model for the evolution of CO WDs relies on the existence of traces of light elements like hydrogen and helium (the former in particular) that survived previous nuclear burnings. Complete stellar models from the main sequence to the WD stages in which the abundances of elements are followed throughout the various nuclear burnings to the values used in this study (i.e.  $X_{\text{H}}$  in the range  $10^{-18}$  to  $10^{-20}$ ) are not presently available. To cope with this, we have presented some plausible arguments to sustain this possibility that eventually has been adopted as a working hypothesis. Null abundances for the light elements in WD interiors cannot be firmly excluded. Stellar models checking this major issue are mandatory.
- Even if our computations rely on state-of-the-art WD

models, the correct approach would be to calculate and follow in time stellar models responding to the new source of energy in the course of evolution. The present models, although acceptable for very low nuclear rates, fail to represent the real physical structure of a WD in presence of large energy production. The WD structure may be deeply altered and follow a different evolutionary history that is not easy to foresee at present.

- Our calculations do not take into account yet the additional energy release due to elements stratification, solid state transition (latent heat) and gravitational contraction.

- Only complete, self-consistent models would allow us to correctly determine the amount of energy generated by nuclear reactions, and to deal with the energy transport problem, rigorously comparing production versus transport of energy.

Future work should be the computation of a self-consistent model able to respond to changing physical conditions, indicating the exact age at which the under-barrier reactions become important and the structural response of a WD to the novel energy input. After the WD cools to the temperature for the activation of the under-barrier channel in the liquid/solid phase, we foresee three possible scenarios: (a) reheating with consequent increase of the cooling lifetime; (b) rejuvenation to another type of object; (c) explosion as type Ia SNa (or a different type?).

We urge reconsidering the whole subject of nuclear reactions in these extreme conditions, in particular in presence of impurities that could deeply change our current understanding of the energy sources in WDs.

*If the results of our exploratory project are confirmed by further investigation, important implications for the currently accepted scenario for type Ia SNe will follow. The binary origin of type Ia SNa explosion would be no longer strictly necessary. Isolated WDs with masses well below the Chandrasekhar limit may reach the threshold for pycno-nuclear burning and consequent SNa explosion due to the survival of traces of light elements. These impurities may remain inactive for long periods of time and be activated only when the WDs reach the liquid-solid regime. Owing to the large range of WD masses that could be affected by the presence of impurities and undergo thermal runaway and consequent SNa explosion, the nature of standard candle so far attributed to type Ia SNe may not be true. Because of the far reaching implications, the whole subject deserves careful future investigation.*

## ACKNOWLEDGEMENTS

We would like to deeply thank Dr. Maurizio Salaris for his friendship, for the many illuminating discussions, and for providing us his cooling sequences and WD models. We like to thank Drs. S. Ichimaru and H. Kitamura for patiently replying to the numberless emails sent by PT and the many very useful explanations and comments. We acknowledge the critical discussion with Dr. K. Shen and finally, the very helpful comments of the unknown referee.

## REFERENCES

- Althaus L. G., Benvenuto O. G., 1997, *ApJ*, 477, 313
- Althaus L. G., Benvenuto O. G., 1998, *MNRAS*, 296, 206
- Althaus L. G., García-Berro E., Isern J., Córscico A. H., Miller Bertolami M. M., 2012, *A&A*, 537, A33
- Althaus L. G., Miller Bertolami M. M., Córscico A. H., 2013, *A&A*, 557, A19
- Althaus L. G., Panei J. A., Miller Bertolami M. M., García-Berro E., Córscico A. H., Romero A. D., Kepler S. O., Rohrmann R. D., 2009, *ApJ*, 704, 1605
- Beard M. L., 2010, PhD thesis, University of Notre Dame
- Bergeron P., Wesemael F., Fontaine G., Liebert J., 1990, *ApJL*, 351, L21
- Bertelli G., Bressan A., Chiosi C., Fagotto F., Nasi E., 1994, 106, 275
- Bertelli G., Girardi L., Marigo P., Nasi E., 2008, *A&A*, 484, 815
- Bertelli G., Nasi E., Girardi L., Marigo P., 2009, *A&A*, 508, 355
- Bressan A., Marigo P., Girardi L., Salasnich B., Dal Cero C., Rubele S., Nanni A., 2012, *MNRAS*, 427, 127
- Brown L. S., Sawyer R. F., 1997, *Reviews of Modern Physics*, 69, 411
- Canuto V., 1970, *ApJ*, 159, 641
- Catalán S., Isern J., García-Berro E., Ribas I., 2008, *MNRAS*, 387, 1693
- Chandrasekhar S., 1939, *An introduction to the study of stellar structure*
- Chiosi C., Bertelli G., Bressan A., 1992, *ARA&A*, 30, 235
- Córscico A. H., Althaus L. G., 2014, *ApJL*, 793, L17
- Dewitt H., Slattery W., Baiko D., Yakovlev D., 2001, *Contributions to Plasma Physics*, 41, 251
- DeWitt H. E., Slattery W. L., Yang J., 1992, in *International Conference on the Physics of Strongly Coupled Plasmas*, Rochester, NY, 17-21 Aug. 1992 Monte Carlo simulation of the OCP freezing transition. pp 17-21
- Eisenstein D. J., Liebert J., Harris H. C., Kleinman S. J., Nitta A., Silvestri N., Anderson S. A., Barentine J. C., Brewington H. J., Brinkmann J., Harvanek M., Krzesiński J., Neilsen Jr. E. H., Long D., Schneider D. P., Snedden S. A., 2006, *ApJS*, 167, 40
- Fowler W. A., Caughlan G. R., Zimmerman B. A., 1975, *ARAA*, 13, 69
- Fujimoto M. Y., 1982a, *ApJ*, 257, 767
- Fujimoto M. Y., 1982b, *ApJ*, 257, 752
- Gasques L. R., Afanasjev A. V., Aguilera E. F., Beard M., Chamon L. C., Ring P., Wiescher M., Yakovlev D. G., 2005, *PhRvC*, 72, 025806
- Hubbard W. B., Lampe M., 1969, *ApJS*, 18, 297
- Iben Jr. I., 1968, *ApJ*, 154, 557
- Iben Jr. I., 1975, *ApJ*, 196, 549
- Iben Jr. I., 2013a, *Stellar Evolution Physics, Volume 1: Physical Processes in Stellar Interiors*
- Iben Jr. I., 2013b, *Stellar Evolution Physics, Volume 2: Advanced Evolution of Single Stars*
- Iben Jr. I., MacDonald J., 1985, *ApJ*, 296, 540
- Iben Jr. I., Renzini A., 1983, *ARA&A*, 21, 271
- Ichimaru S., 1982, *Reviews of Modern Physics*, 54, 1017
- Ichimaru S., Kitamura H., 1999a, *Physics of Plasmas*, 6, 2649
- Ichimaru S., Kitamura H., 1999b, *Physics of Plasmas*, 6, 2649
- Ichimaru S., Ogata S., van Horn H. M., 1992, *ApJL*, 401, L35
- Kawaler S. D., 1988, *ApJ*, 334, 220
- Kepler S. O., Kleinman S. J., Nitta A., Koester D., Castanheira B. G., Giovannini O., Althaus L., 2007, in *Napiwotzki R., Burleigh M. R., eds, 15th European Workshop on White Dwarfs Vol. 372 of Astronomical Society of the Pacific Conference Series, The White Dwarf Mass Distribution*. p. 35
- Kippenhahn R., Weigert A., 1990, *Stellar Structure and Evolution*
- Kitamura H., 2000, *ApJ*, 539, 888
- Kitamura H., Ichimaru S., 1995, *ApJ*, 438, 300
- Lindemann F. A., 1910, *Z. Phys.*, 11, 609
- Mannucci F., Della Valle M., Panagia N., 2006, *MNRAS*, 370, 773
- Marigo P., 2001, *A&A*, 370, 194
- Mestel L., 1952a, *MNRAS*, 112, 583
- Mestel L., 1952b, *MNRAS*, 112, 598
- Miller Bertolami M. M., Althaus L. G., García-Berro E., 2013, *ApJL*, 775, L22
- Napiwotzki R., Christlieb N., Drechsel H., Hagen H.-J., Heber U., Homeier D., Karl C., Koester D., Leibundgut B., Marsh T. R., Moehler S., Nelemans G., Pauli E.-M., Reimers D., Renzini A., Yungelson L., 2003, *The Messenger*, 112, 25
- Nomoto K., 1982a, *ApJ*, 257, 780
- Nomoto K., 1982b, *ApJ*, 253, 798
- Nomoto K., Kobayashi C., Tominaga N., 2013, *ARA&A*, 51, 457
- Ogata S., Iyetomi H., Ichimaru S., 1991, *ApJ*, 372, 259
- Orío M., 2013, *The Astronomical Review*, 8, 010000
- Panei J. A., Althaus L. G., Chen X., Han Z., 2007, *MNRAS*, 382, 779
- Renedo I., Althaus L. G., Miller-Bertolami M. M., Romero A. D., Córscico A. H., Rohrmann R. D., García-Berro E., 2010, *ApJ*, 717, 183
- Salaris M., Althaus L. G., García-Berro E., 2013, *A&A*, 555, A96
- Salaris M., Cassisi S., Pietrinferni A., Kowalski P. M., Isern J., 2010, *ApJ*, 716, 1241
- Salpeter E. E., van Horn H. M., 1969, *ApJ*, 155, 183
- Scalzo R. A., Ruiter A. J., Sim S. A., 2014, *ArXiv e-prints*, 1408.6601
- Schramm S., Koonin S. E., 1990, *ApJ*, 365, 296
- Shapiro S. L., Teukolsky S. A., 1983, *Black holes, white dwarfs, and neutron stars: The physics of compact objects*
- Spergel D. N., Verde L., Peiris H. V., Komatsu E., Nolta M. R., Bennett C. L., Halpern M., Hinshaw G., Jarosik N., Kogut A., Limon M., Meyer S. S., Page L., Tucker G. S., Weiland J. L., Wollack E., Wright E. L., 2003, *ApJS*, 148, 175
- Trimble V., Aschwanden M. J., 2004, *PASP*, 116, 187
- Tsebrenko D., Soker N., 2014a, *ArXiv e-prints*, 1407.6231
- Tsebrenko D., Soker N., 2014b, *ArXiv e-prints*, 1409.0780
- van Horn H. M., 1968, *ApJ*, 151, 227
- Weidemann V., 1967, *Z. Astrophys.*, 67, 286
- Weidemann V., 1977, *A&A*, 59, 411
- Weidemann V., 1990, *ARA&A*, 28, 103
- Weidemann V., 2000, *A&A*, 363, 647

Weiss A., Hillebrandt W., Thomas H.-C., Ritter H., 2004,  
Cox and Giuli's Principles of Stellar Structure  
Yakovlev D. G., Gasques L. R., Afanasjev A. V., Beard M.,  
Wiescher M., 2006, PhRvC, 74, 035803